University of Crete, Department of Physics

FO.R.T.H., Institute of Electronic Structure and Lasers

Master Thesis

Cavity-enhanced atomic Iodine spectroscopy: Towards PNC optical rotation measurements

Name: Toutoudaki Eirini

Supervisor: Prof. T. Peter Rakitzis

Heraklion, 2021

Contents

List of Figures

Acknowledgements

I would like to acknowledge the following people who contributed in their own way to this work, without whom I would not have succeeded.

First, I would like to thank my supervisor Prof. T. P. Rakitzis. I am grateful that I was given the opportunity to work in his team. As a supervisor, he was always there sharing his knowledge and providing guidance throughout this year. I always admired his unique way of thinking, which has redefined my own understanding in physics.

I would also like to thank the rest of the team members, M. Xygkis and Dr. A. Spiliotis, for our great collaboration and the friendly environment they created from the beginning. I would especially like to thank M. Xygkis as we did a lot of this work together.

Finally, and most importantly, I feel a deep sense of gratitude towards Dr. George Katsoprinakis. None of these would be possible without him. He is not only a great scientist but also a wonderful person, and I am very glad working next to such a talented and gifted individual.

I would like to thank all my friends, Fereniki, Maria, Eirini, Kelly, and Marianna who were close to me all the time, supporting and providing help when needed.

Finally, I would like to thank my family, my mother Eleni, my father Nikos, and my brother John for their support and trust all these years.

Abstract

This work presents a cavity-enhanced scheme for the measurement of the atomic iodine spectrum, comprising a four-mirror bow-tie cavity, which increases the effective interaction pathlength of iodine atoms with light, by a factor – essentially – equal to the average number of intracavity photon round-trips.

It also doubles as the first steps towards a new type of atomic parity non-conservation (PNC) experiment. In 1959, Zel'dovich first considered the possibility of measuring PNC in atomic transitions, and suggested that if a parity violating weak neutral-current interaction between the electron and the nucleus exists, then the interference with a parity conserving electromagnetic interaction between the electron and the nucleus would make the atomic system optically active. So, the ability to perform measurements of circular birefringence with high sensitivity would constitute a way to measure PNC in a low-energy, atomic physics experiment.

The Standard Model, predicts a weak parity non-conserving transition amplitude $E1_{PNC}$ between states of the same parity in certain atomic and molecular systems. Measurement of the $E1_{PNC}$ transition amplitude is possible through the interference with the amplitude of a parity allowed transition. In the vicinity of a parity-allowed magnetic-dipole M1 transition, the interference M1-$E1_{PNC}$ leads to natural optical activity.

As a PNC candidate, iodine offers a number of advantages: a high atomic number, *Z*, which enhances the PNC effect, a strong M1 transition with which the PNC amplitude can interfere, readily available means to create significant atomic populations, even at room temperature, a large number of isotopes, where combined measurements can eliminate deficiencies in our theoretical understanding of atomic iodine, the ability to directly compare results with the best-to-date atomic PNC experiment, that on cesium performed by the C.E. Wieman group in the late 1990s, and more. The main aim of this thesis is to study the iodine magnetic-dipole, M1, transition $5^2P_{1/2} \rightarrow 5^2P_{3/2}$ at 1315 nm, and to measure, for the first time, the electric quadrupole E2 component between the same states, which is expected to provide unambiguous information about a specific component of the PNC interaction, that owing to the elusive *anapole moment* of the nucleus. The cavity enhancement outlined above is expected to allow for the study of very small signals, such as PNC optical rotation.

As a further means of enhancement, we also study the effects of increased temperature for the production of higher atomic iodine column densities, in order to maximize the PNC signal.

Περίληψη

Αυτή η εργασία παρουσιάζει μια ενισχυμένη εικόνα μέσω κοιλότητας για την μέτρηση του ατομικού φάσματος ιωδίου, περιλαμβάνει μια κοιλότητα τύπου bow-tie τεσσάρων κατόπτρων, η οποία αυξάνει το ενεργό μήκος αλληλεπίδρασης των ατόμων ιωδίου με το φως, κατά παράγοντα ίσο με τον μέσο αριθμό περασμάτων μέσα στην κοιλότητα.

Επίσης, παρουσιάζονται τα πρώτα βήματα για πειράματα παραβίασης της συμμετρίας της ομοτιμίας (PNC). Το 1959, ο Zel'dovich πρώτος εξέτασε την πιθανότητα μέτρησης PNC σε ατομικές μεταβάσεις και προτάθηκε ότι αν υπάρχει παραβίαση την ομοτιμίας λόγω της ασθενούς αλληλεπίδρασης μεταξύ ηλεκτρονίου και πυρήνα, τότε η συμβολή με μια ηλεκτρομαγνητική αλληλεπίδραση που διατηρεί την ομοτιμία μεταξύ του ηλεκτρονίου και του πυρήνα, αυτό θα έχει σαν αποτέλεσμα το ατομικό σύστημα να γίνεται οπτικά ενεργό. Έτσι, η ικανότητα διεξαγωγής μετρήσεων κυκλικού διχρωισμού με υψηλή ευαισθησία θα αποτελούσε τρόπο μέτρησης του PNC σε πειράματα ατομικής φυσικής χαμηλής ενέργειας.

Το Καθιερωμένο Πρότυπο, προβλέπει μια ασθενή μετάβαση που παραβιάζει την ομοτιμία με πλάτος $E1_{PNC}$ μεταξύ καταστάσεων με όμοια ομοτιμία σε συγκεκριμένα ατομικά και μοριακά συστήματα. Η μέτρηση του πλάτους μετάβασης $E1_{PNC}$ είναι δυνατή μέσω της συμβολής με μία μετάβαση η οποία δε παραβιάζει την ομοτιμία. Στην περίπτωση μια επιτρεπόμενης μαγνητο-διπολικής μετάβασης M1, η συμβολή M1-$E1_{PNC}$ θα οδηγήσει σε φυσική οπτική ενεργότητα.

Σαν υποψήφιο ατομικό σύστημα για PNC, το ιώδιο προσφέρει πολλά πλεονεκτήματα όπως: μεγάλο ατομικό αριθμό, Z, το οποίο ενισχύει το φαινόμενο PNC, ισχυρή M1 μετάβαση με την οποία η μετάβαση $E1_{PNC}$ μπορεί να συμβάλει, εύκολη δημιουργία ατομικών πληθυσμών ακόμη και σε θερμοκρασία δωματίου, μεγάλος αριθμός ισοτόπων, όπου συνδυαστικές μετρήσεις μπορούν να εξαλείψουν ελλείψεις στην θεωρητική κατανόηση του ατομικού ιωδίου, την ικανότητα να συγκρίνουμε άμεσα τα αποτελέσματα με το πιο πρόσφατο ατομικό πείραμα PNC, στο κέσιο όπου πραγματοποιήθηκε από την ομάδα του C.E. Wieman τα τέλη της δεκαετίας του 1990, και άλλα. Ο κύριος στόχος αυτής της εργασίας είναι να μελετηθεί η μαγνητο-διπολική μεταβαση (M1) του ιωδίου, $5^2P_{1/2} \rightarrow 5^2P_{3/2}$ στα 1315 nm και να μετρηθεί, για πρώτη φορά, η ηλεκτρο-τετραπολική συνιστώσα E2 μεταξύ των ίδιων καταστάσεων, το οποίο αναμένεται να παρέχει πληροφορίες σχετικές με μια συγκεκριμένη συνιστώσα της PNC αλληλεπίδρασης, το οποίο οφείλεται στην αναπολική ροπή του πυρήνα. Η ενίσχυση μέσω οπτικής κοιλότητας που περιγράφεται, αναμένεται να επιτρέψει την μελέτη πολύ μικρών σημάτων, όπως η οπτική περιστροφή λόγω PNC.

Ως ένα περαιτέρω μέσο ενίσχυσης, μελετάμε την επίδραση της αύξησης της θερμοκρασίας για την παραγωγή μεγαλύτερων ατομικών πυκνοτήτων, με στόχο την μεγιστοποίηση του σήματος PNC.

Chapter 1: Cavities

1.1 Basics of cavities

An optical cavity is an arrangement of mirrors that forms a standing wave cavity resonator for light waves. Optical cavities are a major component of lasers, surrounding the gain medium and providing feedback of the laser light. They are also used in optical parametric oscillators and some interferometers. Light confined in the cavity reflects multiple times, producing standing waves for certain resonance frequencies. The standing wave patterns produced are called *modes*; longitudinal modes (of the same order) differ only in resonant frequency, but maintain the same spatial intensity profile, while transverse modes differ in both frequency, and intensity profile across the cross-section of the beam.

The most common types of optical cavities consist of two facing plane (flat) or spherical mirrors. The simplest of these is the plane-parallel or Fabry–Pérot cavity, consisting of two opposing flat mirrors.

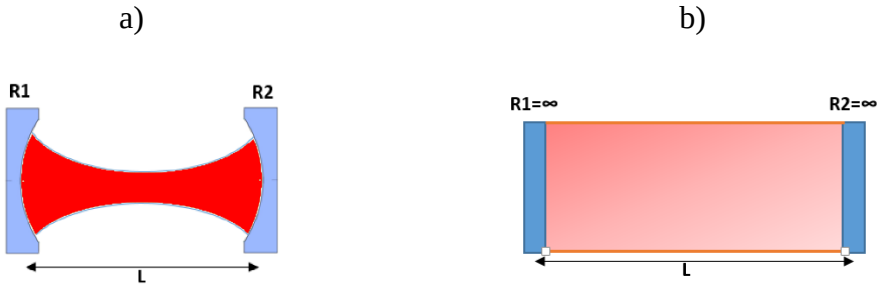

Figure 1: a) Spherical mirror cavity and b) Fabry – Pérot cavity.

1.2 Cavity Resonances

The resonance of an electromagnetic wave inside an optical cavity is no different than the resonance of any other system. To make the problem as familiar as possible, we consider the cavity shown in Figure 2. We consider incident on the cavity all the waves, from the left, inside the cavity, or transmitted through it to the right to be plane waves.

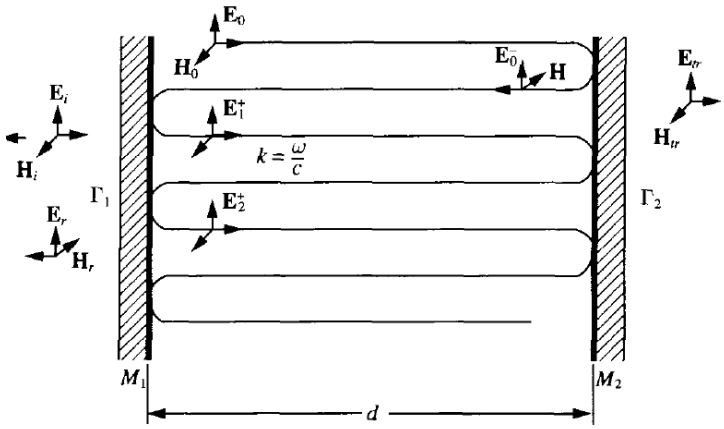

Figure 2: Optical cavity. Image from Verdeyen – Laser Electronics [1]

Let suppose that we have a wave as it bounces back and forth between the two mirrors. Consider $\mathbf{E_0}$ to be the initial field to the right if M_1. It propagates to M_2 and back to M_1 and experiences an amplitude change of $\Gamma_1 \cdot \Gamma_2$ and a phase factor $e^{[-j\,k2d]}$ as it travels between the two mirror, and thus generates the field $\mathbf{E_1^+}$, which experiences the same changes as $\mathbf{E_0}$, and in turn generates $\mathbf{E_2^+}$, and so on. All the fields that are generated at every point along M_1 to M_2 ($\mathbf{E_1^+}$, $\mathbf{E_2^+}$, and so on), must be added to the initial field $\mathbf{E_0}$, which we define to have the reference phase of 0°. We have assumed that the *round trip phase shift* (RTPS), $2\theta = 2kd$, is almost an integral multiple of 2π radians. That deficiency is labeled by φ and is related to *kd* by

$$2\theta = 2kd - \varphi \tag{1.1}$$

where q is an integer.

By assuming that $\varphi = 0$, we define the resonance condition as

$$k \cdot 2d = \frac{\omega n \cdot 2d}{c} = \frac{2\pi \cdot 2d}{\lambda} = q \cdot 2\pi \tag{1.2}$$

Or

$$d = \frac{q \cdot \lambda}{2} \tag{1.3}$$

where $\lambda = \frac{\lambda_0}{n}$. This view of resonance states that there has to be an integral number of half wavelengths between the two mirrors, or, more generally, an integral number of wavelengths along the total cavity round-trip length.

1.3 Important Quantities

The frequency difference between successive modes of the cavity is important and is called *Free Spectral Range* (FSR). Equation *(1.2)* can also be interpreted in terms of frequency *f* as:

$$k \cdot 2d = \omega\,\frac{2nd}{c} = 2\pi f \cdot \frac{2nd}{c} = q \cdot 2\pi \Rightarrow$$

$$f = q \cdot \frac{c}{2nd} \tag{1.4}$$

Because q is restricted to integer values, there are only discrete frequencies which obey the resonance condition. The separation between those frequencies is given by

$$f_{q+1} - f_q = \frac{c}{2nd} = FSR \tag{1.5}$$

There are three interrelated characteristic parameters associated with a cavity that describe the resonance phenomenon: *Q* (*quality factor*), *F* (*finesse*), and τ_p (*photon lifetime*). To derive an explicit relationship between the resonance, these quantities, and the characteristics of the cavity, we need an analytic description of the fields inside the cavity and their relationship to those exciting the cavity. After some mathematical operations we obtain a generic expression for the power transmission through an arbitrary cavity with reflection coefficients of the input and output mirrors, R_{in} and R_{out}, respectively, and $A = \sqrt{R_{in}R_{out}(1 - \text{cavity losses})}$, the *per round-trip survival factor* of the cavity:

$$T(f) = \frac{(1 - R_{in})(1 - R_{out})}{(1 - A)^2} \frac{1}{1 + \left(\frac{2F}{\pi}\right)^2 \sin^2(2\,\pi\,(f - f_q)\,L/c)} \tag{1.6}$$

where f_q the cavity resonant frequencies, and F the finesse defined below.

A plot of the transmission coefficient *(1.6)* versus the frequency f is shown in Figure 3 for different reflection coefficients R_{in}, R_{out}.

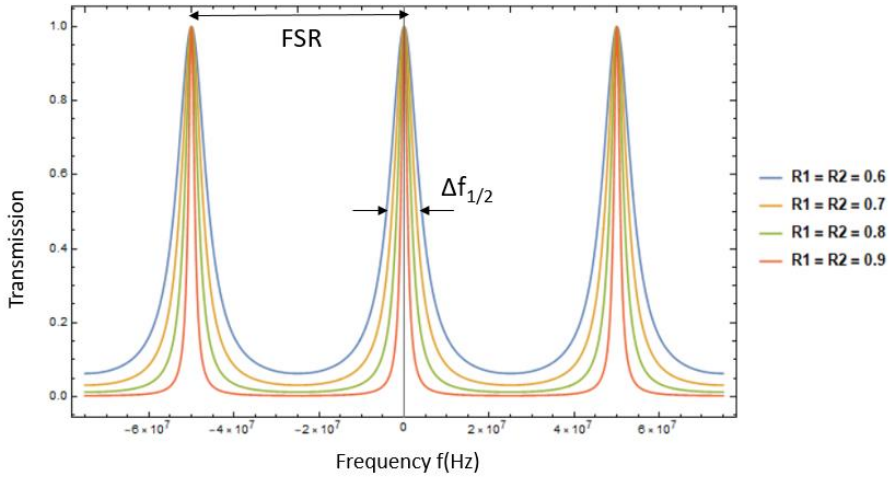

Figure 3: Transmission through a Fabry - Perot cavity as a function of the frequency for various reflection coefficients.

The *quality factor* (Q) of the cavity is a measure of the sharpness or selectivity of the resonance. If f_0 is the frequency of one of the peaks, then Q is given by:

$$Q = \frac{f_0}{\Delta f_{1/2}} = \frac{\omega_0}{\Delta \omega_{1/2}} = \frac{\lambda_0}{\Delta \lambda_{1/2}} \tag{1.7}$$

where $\Delta f_{1/2}$ is the *full width at half of the maximum* (FWHM) of the cavity resonance, in frequency units, given by:

$$\Delta f_{1/2} = \frac{FSR}{\pi}\left\{\frac{1 - A}{\sqrt{A}}\right\} \tag{1.8}$$

Thus,

$$Q = \frac{q(c/2nd)}{\Delta f_{1/2}} = \frac{2\pi nd}{\lambda_0}\frac{\sqrt{A}}{1 - A} \tag{1.9}$$

The Finesse (F), appearing in *(1.6)*, is defined as

$$F = \frac{FSR}{FWHM} = \frac{FSR}{\Delta f_{1/2}} \tag{1.10}$$

Or,

$$F = \frac{\pi\sqrt{A}}{1 - A} \tag{1.11}$$

1.4 Alignment and mode matching

Proper *mode matching* between an input laser beam and an optical cavity means that the laser beam couples completely, in both shape and path, to the fundamental (longitudinal) spatial mode (TEM_{00q}) of the cavity and not at all to the higher-order (off-axis) spatial modes (TEM_{lmq}). In Figure 4 we see the spectrum of the cavity which supports higher-order modes. In this section we will show the conditions that will allow us to have only the first transverse mode (TEM_{00q}).

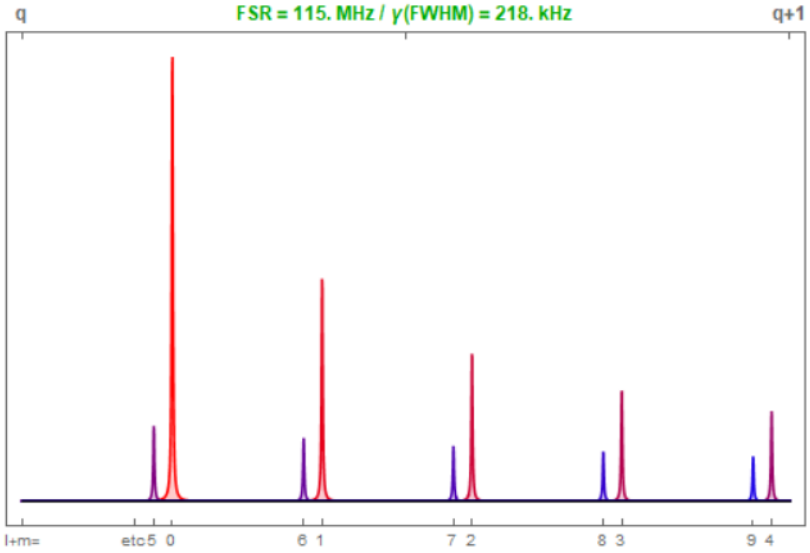

Figure 4: Transmittance of the cavity with higher-order spatial modes (TEM_{mnq}).

In one dimension, the normalized spatial eigenmodes are Hermite-Gaussians, the first order is given by:

$$U_0(x) = \left(\frac{2}{\pi x_0^2}\right)^{1/4} e^{-\left(\frac{x}{x_0}\right)^2} \tag{1.12}$$

where x_0 is called the waist size. For a two spherical (radius R_1 and R_2) mirrored cavity of mirror spacing d,

$$x_0^4 = \left(\frac{\lambda}{\pi}\right)^2 \frac{d(R_1 - d)(R_2 - d)(R_1 + R_2 - d)}{(R_1 + R_2 - 2d)^2} \tag{1.13}$$

We begin with the assumption that the input beam $\Psi(x)$ is a Gaussian and aligned, so that $\Psi(x) = AU_0(x)$ and then see what happens as it is misaligned. If we translate the input beam by a small amount, a_x, $\Psi(x)$ becomes:

$$\begin{aligned} \Psi(x) &= AU_0(x - a_x) \\ &= A\left(\frac{2}{\pi x_0^2}\right)^{1/4} e^{-\left(\frac{x - a_x}{x_0}\right)^2} \end{aligned} \tag{1.14}$$

The exponential can be expanded and if $\frac{a_x}{x_0} \ll 1$ and equation *(1.14)* can be rewritten as:

$$\Psi(x) \simeq A\left(\frac{2}{\pi x_0^2}\right)^{\frac{1}{4}} \left(1 + 2a_x \frac{x}{x_0^2}\right) e^{-\left(\frac{x}{x_0}\right)^2} \tag{1.15}$$

Or

$$\Psi(x) \simeq A(U_0(x) + \frac{a_x}{x_0} U_1(x) \tag{1.16}$$

Where

$$U_1(x) = \left(\frac{2}{\pi x_0^2}\right)^{1/4} \frac{2x}{x_0} e^{-\left(\frac{x}{x_0}\right)^2}$$

is the second spatial mode. Thus we see that a small displacement of the input beam gives rise to a coupling of the first off-axis mode of the cavity.

The last case to be treated is that in which the beam size is correctly matched, but the position of the waist is not. To describe what happens when the input waist is displaced a distance *b* along the cavity axis *z* from the cavity waist, we rewrite the two lowest-order modes as

$$V_0(r,z) = \sqrt{\frac{2}{\pi}} \frac{1}{w} e^{\left(-r^2\left(\frac{1}{w^2} + i\frac{\pi}{\lambda R}\right)\right)} \tag{1.17}$$

$$V_1(r,z) = \sqrt{\frac{2}{\pi}} \frac{1}{w} \left(1 - 2\frac{r^2}{w^2}\right) e^{\left(-r^2\left(\frac{1}{w^2} - i\frac{\pi}{\lambda R}\right)\right)} \tag{1.18}$$

Where *R* is the radius of curvature which given by:

$$R(z) = z\left(1 + \left(\pi \frac{w_0^2}{\lambda z}\right)^2\right) \tag{1.19}$$

And *w* is the spots size of the eigenmodes and varies as

$$w^2(z) = w_0^2 \left(1 + \left(\frac{\lambda z}{\pi w_0^2}\right)^2\right) \tag{1.20}$$

The distance *z* is measured from the cavity waist, at a short distance *b* from the waist we assume that:

$$\left(\frac{\lambda b}{\pi w_0^2}\right) \ll 1$$

$$w^2(b) = w_0^2$$

Hence, the axially translated input beam at the cavity waist takes the form:

$$\Psi(r,b) = A\sqrt{\frac{2}{\pi}} \frac{1}{w} \left(1 - 2\frac{r^2}{w^2}\right) e^{\left(\frac{-r^2}{w_0^2}\left(1 - i\frac{\lambda b}{\pi w_0^2}\right)\right)} \tag{1.21}$$

Finally, expanding the exponential, the beam in terms of eigenmodes is:

$$\Psi(r,z) = A(V_0 + i\frac{\lambda b}{2\pi w_0^2} V_1) \tag{1.22}$$

So, we see that an axial displacement of the input waist causes a coupling to higher-order radial eigenmodes. The way to overcome this is to use lenses in the right positions, in order to match the beam waist with the cavity waist [2].

1.5 Cavity-enhanced polarimetry

In optics, polarized light is usually described using either the Mueller or the Jones calculus. We use the latter, derived by R. C. Jones in 1941. Polarized light is represented by a 2D Jones vector, and linear optical elements are represented by 2×2 Jones matrices. When light traverses an optical element the resulting polarization of the emerging light is found by taking the product of the Jones matrix of the optical element and the Jones vector of the incident light. Note that Jones calculus is only applicable to light that is already fully polarized. Light which is randomly polarized, partially polarized, or incoherent must be treated using the Mueller calculus.

The Jones matrix of an optically active element (circularly birefringent optical rotator) is an SU(2) rotation matrix with argument θ:

$$R_c(\theta) = \begin{pmatrix} \cos\theta & -\sin\theta \\ \sin\theta & \cos\theta \end{pmatrix} \tag{1.23}$$

Anisotropies such as imperfections of transmission optics, thermal or stress-induced birefringences, and stray magnetic fields can be described as linearly birefringent optical elements. The Jones matrix for a general linear wave retarder, which introduces a differential phase shift δ, is given by

$$R_l(\delta) = \begin{pmatrix} e^{i\delta/2} & 0 \\ 0 & e^{-i\delta/2} \end{pmatrix} \tag{1.24}$$

The cavity round-trip Jones matrices for the propagation are obtained by the ordered multiplication of the Jones matrices representing the optical elements. The round-trip Jones matrices are given by

$$R = R_e(\delta) \cdot R_c(\theta) \tag{1.25}$$

The eigen-polarizations of the cavity modes, along with their respective resonance frequencies, are determined by the anisotropies of the cavity. Using the explicit form of the transfer matrices, we can obtain the eigensystem as a function of the parameters (θ, δ).

The matrix R has two eigenvalues and two eigenvectors. The eigenvectors are generally complex, orthogonal vectors $v_\pm$ and represent the eigenpolarizations of each cavity mode. The eigenvalues can be written in the form $\lambda_\pm = e^{\pm i\varphi}$. The phase of each eigenvalue is the round-trip optical phase shift obtained during light propagation and therefore yields the frequency splitting of the eigenmodes. Expanding *(1.25)*, we obtain

$$R = \begin{pmatrix} e^{\frac{i\delta}{2}}\cos(\theta) & -\sin(\theta) \\ \sin(\theta) & e^{-\frac{i\delta}{2}}\cos(\theta) \end{pmatrix} \tag{1.26}$$

The eigenvalues and eigenvectors are:

$$\lambda^{\pm} = \cos(\theta)\cos\left(\frac{\delta}{2}\right) \mp i\sqrt{1-\cos^2\theta\cos\left(\frac{\delta}{2}\right)^2} \tag{1.27}$$

$$\nu^{\pm} = A\begin{pmatrix}\csc(\theta)\left(\cos(\theta)\sin\left(\frac{\delta}{2}\right) \mp \sqrt{1-\cos^2\theta\cos\left(\frac{\delta}{2}\right)^2}\right)\\ -i\end{pmatrix} \tag{1.28}$$

Where A is a normalization constant which is functions of θ and δ. We see that in the most general case the polarization eigenstates are represented by orthogonal ellipses and their frequency splitting is proportional to $\Gamma = \cos^{-1}(\cos(a)\cos(\frac{\delta}{2}))$ [3]

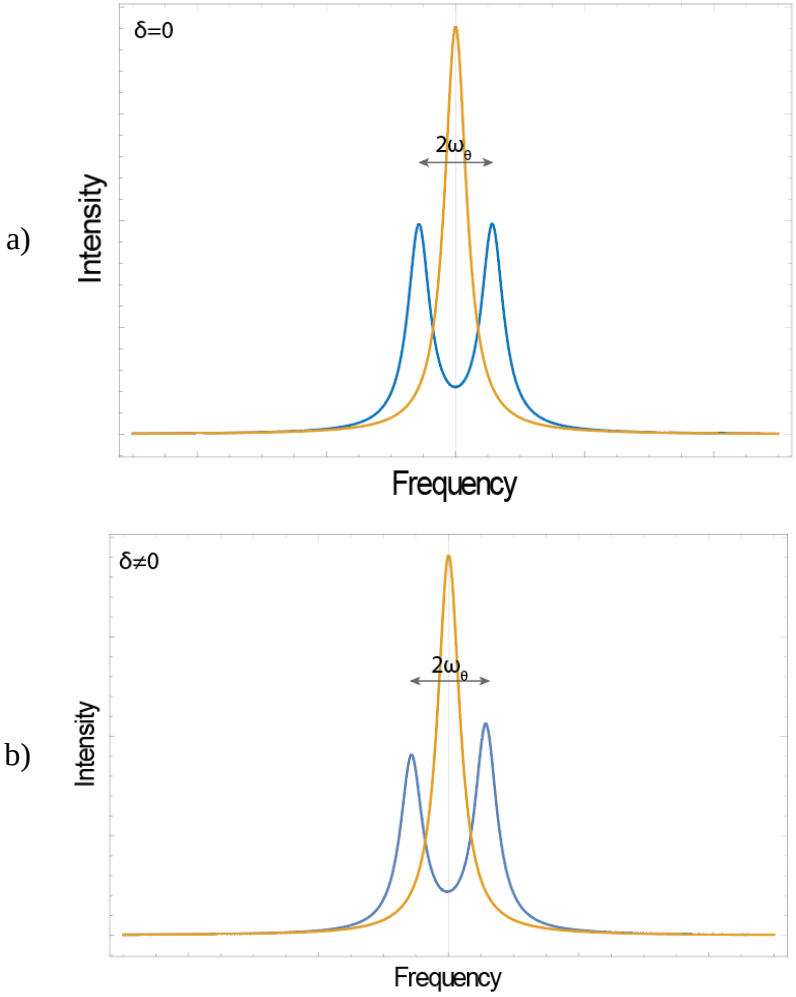

Figure 5: Optical activity (circular birefringence) splits the eigenmodes (blue lines) by $2\omega_\theta = 2\theta c/L$. a) We see the splitting without linear birefringence and b) in the presence of linear birefringence, the eigenmodes transforms into elliptical states. The orange line corresponds to the degenerate axial mode of an isotropic cavity.

In the context of this thesis, we operate on cavities in the absence of both circular, as well as linear birefringence, as our goal is to study the absorption from atomic iodine vapor. Thus, our cavity spectrum comprises degenerate resonances for any incoming light polarization.

However, the treatment above encompasses our future plans for studying effects owing to circular birefringence inside our optical cavities, namely Faraday rotation due to applied magnetic fields on the atomic vapor, and, ultimately, the weak chiral optical activity due to the non-conservation of parity in the specific iodine transitions under study.

Chapter 2: Multipole Transitions

2.1 Maxwell's Equations

The two fundamental quantities defining the electromagnetic field are the electric $\mathbf{E}(\boldsymbol{r},t)$ and magnetic $\mathbf{H}(\boldsymbol{r},t)$ fields which are functions of space and time satisfying the Maxwell's equations. In the nonrelavistic form and SI units, they are given by,

$$\boldsymbol{\nabla}\times\mathbf{E}+\frac{\partial\mathbf{B}}{\partial \mathrm{t}}=0 \tag{2.1}$$

$$\boldsymbol{\nabla}\times\mathbf{H}+\frac{\partial\mathbf{D}}{\partial \mathrm{t}}=\mathbf{J} \tag{2.2}$$

$$\boldsymbol{\nabla}\cdot\mathbf{D}=\sigma \tag{2.3}$$

$$\boldsymbol{\nabla}\cdot\mathbf{B}=0 \tag{2.4}$$

where J and σ are the densities of currents and free charges, respectively, while $\boldsymbol{D}=\varepsilon_0\boldsymbol{E}$ and $\boldsymbol{B}=\mu_0\boldsymbol{H}$ with ε_0 the electric permittivity and μ_0 the magnetic permeability of vacuum. The fields can be expressed in terms of the scalar $\varphi(\boldsymbol{r},t)$ and vector $\mathbf{A}(\boldsymbol{r},t)$ potentials as

$$\boldsymbol{E}=-\boldsymbol{\nabla}\varphi-\frac{\partial\boldsymbol{A}}{\partial t},\ \boldsymbol{B}=\boldsymbol{\nabla}\times\boldsymbol{A} \tag{2.5}$$

If we choose $\varphi=0$ and $\boldsymbol{\nabla}\cdot\mathbf{A}=0$, then the fields are given by:

$$\boldsymbol{E}=-\frac{\boldsymbol{\partial A}}{\boldsymbol{\partial t}},\ \boldsymbol{B}=\boldsymbol{\nabla}\times\boldsymbol{A} \tag{2.6}$$

which means than if we know the vector potential $\mathbf{A}(\boldsymbol{r},t)$we can easily obtain the fields. Substituting *(2.6)* into the equation *(2.2)* we obtain

$$\left(\nabla^2-\frac{1}{c^2}\frac{\partial^2}{\partial t^2}\right)\boldsymbol{A}(\boldsymbol{r},t)=0 \tag{2.7}$$

where $c=(\mu_0\varepsilon_0)^{-1/2}$ is the speed of light in vacuum.[4]

2.2 Atom Interacting with EM field

Let us employ time-dependent perturbation theory to investigate the interaction of an atom with classical electromagnetic radiation. It will still be assumed that the particles involved are nonrelativistic. The Hamiltonian of such an atom is:

$$\mathrm{H}=\sum_{\mathrm{i}}\left[\frac{1}{2\mathrm{m_e}}(\widehat{\mathbf{p}_\mathbf{i}}+\mathrm{e}\mathbf{A_i})^2-\mathrm{e}\varphi_\mathrm{i}-\mathrm{g}\frac{\mathrm{e}}{2\mathrm{m_e}}\mathbf{B_i}\cdot\widehat{\mathbf{S}_\mathbf{i}}\right]+\mathrm{V} \tag{2.8}$$

where the sum is over the electrons in the atom. In *(2.8)*, m is the electron's mass, $\widehat{\boldsymbol{p}_\iota}$ its momentum and q its charge, while V is the atomic potential. The remaining terms in *(2.8)* express the effect of the additional external EM field, where $\widehat{\boldsymbol{S}_\iota}$ is the spin of the electrons interacting with the magnetic field. As before, by choosing $\varphi = 0$ and $\boldsymbol{\nabla} \cdot \mathbf{A} = 0$, the Hamiltonian can be rewritten as

$$\mathrm{H} = \mathrm{H}_0 + \sum_{\mathrm{i}} \left[\frac{\mathrm{e}}{\mathrm{m_e}} \mathbf{A_i} \cdot \hat{\mathbf{p}}_{\mathrm{i}} + \frac{\mathrm{e}^2}{2\mathrm{m_e}} \mathbf{A_i^2} + \mathrm{g} \frac{\mathrm{e}}{2\mathrm{m}} \mathbf{B_i} \cdot \widehat{\mathbf{S}_\mathbf{i}} \right] \tag{2.9}$$

The term H_0 is the Hamiltonian of the atom in the absence of the external electromagnetic field. Note that $\widehat{\boldsymbol{p}}$ and $\mathbf{A}$ commute because $\boldsymbol{\nabla} \cdot \mathbf{A} = 0$ and the term proportional to $\boldsymbol{A^2}$ can be neglected as it is very small.

Thus, the time-dependent Hamiltonian of a single electron is equal to

$$\mathrm{H}_1 = \frac{\mathrm{e}}{\mathrm{m_e}} \mathbf{A} \cdot \hat{\mathbf{p}} - \mathrm{g} \frac{\mathrm{e}}{2\mathrm{m_e}} \mathbf{B} \cdot \hat{\mathbf{S}} = \mathrm{H_e} + \mathrm{H_m} \tag{2.10}$$

From the equations *(2.6)* and *(2.7)* the vector potential $\boldsymbol{A}(\boldsymbol{r}, t)$**,** the electric $\boldsymbol{E}(\boldsymbol{r}, t)$and magnetic $\boldsymbol{B}(\boldsymbol{r}, t)$ fields corresponding to a simple wave can be generalized as

$$\boldsymbol{A} = \widehat{r_e} \frac{E_0}{\sqrt{2} i \omega} e^{i(\boldsymbol{k}\cdot\boldsymbol{r} - \omega t)}, \boldsymbol{E} = \widehat{r_e} \frac{E_0}{\sqrt{2}} e^{i(\boldsymbol{k}\cdot\boldsymbol{r} - \omega t)}, \boldsymbol{B} = -\widehat{r_b} \frac{E_0}{\sqrt{2} C} e^{i(\boldsymbol{k}\cdot\boldsymbol{r} - \omega t)}{}^{1}.$$

The exponential can be expressed as a Taylor series:

$$\mathrm{e}^{\mathrm{i}\mathbf{k}\cdot\mathbf{r}} = \sum_{\mathrm{n}=0}^{\infty} \frac{(\mathrm{i}\mathbf{k}\cdot\mathbf{r})^{\mathrm{n}}}{\mathrm{n}!} = \sum_{\mathrm{l}=1}^{\infty} \frac{(\mathrm{i}\mathbf{k}\cdot\mathbf{r})^{\mathrm{l}-1}}{(\mathrm{l}-1)!} \tag{2.11}$$

This is the *multipole expansion* of the electromagnetic field, where the index $l = n - 1$ is defined to be the *multipole order*.[5]

2.3 Electric Dipole Transitions

The most common simplification of the multipole expansion, which is also the strongest contribution when allowed, is the electric dipole approximation. For the electric dipole approximation we choose the term $l = 1$ in equation *(2.11)* to get $e^{ik\cdot r} \simeq 1$, *i.e.* we consider $k \cdot r \ll 1$, or, equivalently, $r \ll \lambda$, that is the wavelength of the incoming light is much greater than the dimensions of the atom, thus the electron perceives the incoming electric field as an oscillatory field with no spatial dependence Therefore, if we consider a system with initial and final state $|a\rangle$ and $|b\rangle$, respectively, described by the Hamiltonian H_e we can calculate the electric dipole matrix element

[1] $\boldsymbol{k} = \hat{n}k$, $\hat{n} = \hat{r_e} \times \hat{r_b}$, $\hat{r_e} \cdot \hat{r_b} = 0$

$$H_{ab}^{E1} = \langle a|H_e|b\rangle = \langle a|\frac{e}{m_e}\frac{E_0}{\sqrt{2}i\omega}\boldsymbol{p}\cdot\widehat{\boldsymbol{r_e}}|b\rangle = e\frac{E_0}{\sqrt{2}i\omega}\langle a|[H_0, r]\cdot\hat{r}_e|b\rangle \ ^{2} =$$

$$= e\frac{E_0}{\sqrt{2}i\omega} i\omega\langle a|\boldsymbol{r}\cdot\hat{\boldsymbol{r}}_{\boldsymbol{e}}|b\rangle \Longrightarrow$$

$$H_{ab}^{E1} = \frac{E_0}{\sqrt{2}}\langle a|\boldsymbol{D}\cdot\hat{\boldsymbol{r}}_{\boldsymbol{e}}|b\rangle \tag{2.12}$$

where $\boldsymbol{D} = e\cdot\boldsymbol{r}$ is the electric dipole moment and $\widehat{\boldsymbol{D}} = \sum_i e\cdot r_i$ the electric dipole operator. We can proceed further, with the angular part of the matrix element integral

$$H_{ab}^{E1} \approx \langle a|\boldsymbol{D}\cdot\widehat{\boldsymbol{r_e}}|b\rangle = \int_0^\infty r^2 dr R_{n_a l_a}^* R_{n_b l_b} \int d\Omega Y_{l_a m_a}^* \boldsymbol{r}\cdot\hat{r}_e Y_{l_b m_b} \tag{2.13}$$

From the integral in *(2.13)* it follows that the matrix elements are nonzero if

$$\Delta J = J_a - J_b = 0, \pm 1;\ J_a + J_b \geq 1, \tag{2.14}$$

$$\Delta m = m_a - m_b = 0, \pm 1 \tag{2.15}$$

To these selection rules it is necessary to add the selection rule with respect to ***parity***. The components of the electric dipole moment **D**, change sign under inversion. Thus, ***electric dipole transitions are possible only between states of different parity*** (i.e. **even ↔ odd**).[6]

2.4 Electric Quadrupole Transitions

In order to calculate the electric quadrupole matrix element, we choose the $l = 2$ order in equation *(2.11)*. Thus, we have $e^{ik\cdot r} \simeq 1 + i\boldsymbol{k}\cdot\boldsymbol{r}$ and the matrix element is given by

$$H_{ab}^{E2} = \langle a|H_e|b\rangle = \frac{E_0}{\sqrt{2}}\langle a|\boldsymbol{D}\cdot\hat{\boldsymbol{r}}_{\boldsymbol{e}}|b\rangle + \langle a| + \frac{e}{m_e}\frac{E_0}{\sqrt{2}i\omega}(i\boldsymbol{k}\cdot\boldsymbol{r})\hat{\boldsymbol{r}}_{\boldsymbol{e}}\cdot\boldsymbol{p}|b\rangle \tag{2.16}$$

Suppose that the electric dipole transition from state $|a\rangle$ to state $|b\rangle$ is forbidden according to the selection rules in the previous section. This implies that:

$$\langle a|\boldsymbol{D}\cdot\hat{\boldsymbol{r}}_{\boldsymbol{e}}|b\rangle = 0$$

In this case, equation *(2.16)* reduces to

$$H_{ab}^{E2} = \langle a|\frac{e}{m_e}\frac{E_0}{\sqrt{2}i\omega}(i\boldsymbol{k}\cdot\boldsymbol{r})\hat{\boldsymbol{r}}_{\boldsymbol{e}}\cdot\boldsymbol{p}|b\rangle = \frac{e}{m_e}\frac{E_0}{\sqrt{2}\omega}\langle a|\frac{\omega}{c}(\hat{n}\cdot\boldsymbol{r})(\hat{r}_e\cdot\boldsymbol{p})|b\rangle \ ^{3} =$$

$$= \frac{e}{m_e}\frac{E_0}{\sqrt{2}c}\langle a|(\hat{n}\cdot\boldsymbol{r})(\hat{r}_e\cdot\boldsymbol{p})|b\rangle \tag{2.17}$$

Using the definition of the orbital angular momentum $L = \boldsymbol{r}\times\boldsymbol{p}$ we have

---

[2] $[H_0, \boldsymbol{r}] = \frac{\hbar}{i}\frac{\boldsymbol{p}}{m}$

[3] $\boldsymbol{k} = \hat{n}\cdot k = \hat{n}\frac{\omega}{c}$

$$\hat{r_b} \cdot L = (\hat{n} \times \hat{r_e})(\boldsymbol{r} \times \boldsymbol{p}) = (\hat{n} \cdot \boldsymbol{r})(\hat{r_e} \cdot \boldsymbol{p}) - (\hat{r_e} \cdot \boldsymbol{r})(\hat{n} \cdot \boldsymbol{r}) \tag{2.18}$$

Furthermore, if

$$\frac{im_e}{\hbar}[H, (\hat{r_e} \cdot \boldsymbol{r})(\hat{n} \cdot \boldsymbol{r})] = (\hat{r_e} \cdot \boldsymbol{r})(\hat{n} \cdot \boldsymbol{p}) + (\hat{n} \cdot \boldsymbol{r})(\hat{r_e} \cdot \boldsymbol{p}) \tag{2.19}$$

from equations *(2.18)*, *(2.19)* we have,

$$(\hat{n} \cdot \boldsymbol{r})(\hat{r_e} \cdot \boldsymbol{p}) = \frac{1}{2} r_{\mathrm{b}} \cdot \mathrm{L} + \frac{\mathrm{i}m_e}{2\hbar}[H, (\hat{\mathrm{r}}_{\mathrm{e}} \cdot \mathbf{r})(\hat{\mathrm{n}} \cdot \mathbf{r})]$$

which yields

$$H_{ab}^{E2} = \frac{eE_0}{2\sqrt{2}m_e c}\langle a|\boldsymbol{L} \cdot \hat{r_b}|b\rangle + \frac{ieE_0}{2\hbar c}\langle a|[H, (\hat{r_e} \cdot \boldsymbol{r})(\hat{n} \cdot \boldsymbol{r})]|b\rangle =$$

$$\frac{eE_0}{2\sqrt{2}m_e c}\langle a|\boldsymbol{L} \cdot \hat{r_b}|b\rangle + \frac{ieE_0\omega}{2c}\hat{\boldsymbol{r}}_{\boldsymbol{e}} \cdot \boldsymbol{Q_{ab}} \cdot \hat{n} \tag{2.20}$$

Where

$$Q_{ab} = \langle a|\boldsymbol{r_i r_j} - \frac{r^2\delta_{ij}}{3}|b\rangle; r^2 = r_j r_j \tag{2.21}$$

is the *electric quadrupole* operator.

The selection rules for electric quadrupole transitions are given by the second term in equation *(2.20)* when the integral is non-zero. The general form of these selection rules is

$$\Delta J = 0, \pm 1, \pm 2 \quad (0 \nleftrightarrow 0, 1) \tag{2.22}$$

$$\Delta m = 0, \pm 1, \pm 2 \tag{2.23}$$

2.5 Magnetic Dipole Transitions

According to equation *(2.20)*, the first term mediates the magnetic dipole transition between states $|a\rangle$ and $|b\rangle$. However, this expression is incomplete because we neglected taking into account the second term of the Hamiltonian, H_m. Which, indicates the interaction of the magnetic field with the electron's magnetic moment[7]. Taking into account again the first order of the exponential $e^{ik\cdot r} \simeq 1$ we can know define the magnetic dipole matrix element

$$H_{ab}^{M1} = \frac{eE_0}{2\sqrt{2}m_e c}\langle a|\boldsymbol{L} \cdot \hat{r_b}|b\rangle + g\frac{eE_0}{2\sqrt{2}m_e c}\langle a|\hat{r_b} \cdot S|b\rangle \Longrightarrow$$

$$H_{ab}^{M1} = \frac{eE_0}{2\sqrt{2}m_e c}\langle a|(\boldsymbol{L} + \mathrm{g}\mathbf{S}) \cdot \hat{r_b}|b\rangle = \frac{eE_0}{2\sqrt{2}m_e c}\langle a|\mathbf{M_{ab}} \cdot \hat{r_b}|\mathrm{b}\rangle \tag{2.24}$$

Where

$$\boldsymbol{M_{ab}} = \boldsymbol{L} + g\boldsymbol{S} \tag{2.25}$$

is termed the magnetic dipole operator. According to the previous analysis for the electric dipole transition, $\langle a|\mathbf{M_{ab}} \cdot \hat{r_b}|b\rangle$ is non-zero if

$$\Delta L = 0, \tag{2.26}$$

$$\Delta J = 0, \pm 1 \quad (0 \nleftrightarrow 0), \tag{2.27}$$

$$\Delta m = 0, \pm 1 \tag{2.28}$$

2.6 Higher order Transitions

It is obvious that we can choose higher orders of the exponential and that will lead to magnetic quadrupole M2, magnetic octupole M3, electric octupole E3, etc. matrix elements. In the following table we summarize the selection rules for these radiative transitions

Allowed Transitions		*Electric dipole(E1)*	*Magnetic dipole (M1)*	*Electric quadrupole (E2)*	*Magnetic quadrupole (M2)*	*Electric octupole (E3)*	*Magnetic octupole (M3)*
Rigorous rules	(1)	$\Delta J = 0, \pm 1$ $(J = 0 \nrightarrow 0)$		$\Delta J = 0, \pm 1, \pm 2$ $(J = 0 \nrightarrow 0{,}1; \frac{1}{2} \nrightarrow \frac{1}{2})$		$\Delta J = 0, \pm 1 \pm 2, \pm 3$ $(J = 0 \nrightarrow 0{,}1{,}2; \frac{1}{2} \nrightarrow \frac{1}{2}, \frac{3}{2}; 1 \nrightarrow 1)$	
	(2)	$\Delta M_j = 0, \pm 1$		$\Delta M_j = 0, \pm 1 \pm 2$		$\Delta M_j = 0, \pm 1, \pm 2, \pm 3$	
	(3)	$\pi_f = -\pi_i$	$\pi_f = \pi_i$		$\pi_f = -\pi_i$		$\pi_f = \pi_i$
LS coupling	(4)	$\Delta L = \pm 1$	$\Delta L = 0$	$\Delta L = 0, \pm 2$	$\Delta L = \pm 1$	$\Delta L = \pm 1, \pm 3$	$\Delta L = 0, \pm 2$
	(5)	If $\Delta S = 0$ $\Delta L = \pm 1$ $(L = 0 \nrightarrow 0)$	If $\Delta S = 0$ $\Delta L = 0$	If $\Delta S = 0$ $\Delta L = 0, \pm 1, \pm 2$ $(L = 0 \nrightarrow 0{,}1)$		If $\Delta S = 0$ $\Delta L = 0, \pm 1, \pm 2, \pm 3$ $(L = 0 \nrightarrow 0{,}1{,}2; 1 \nrightarrow 1)$	
Intermediate coupling	(6)	If $\Delta S = \pm 1$ $\Delta L = 0, \pm 1, \pm 2$		If $\Delta S = \pm 1$ $\Delta L = 0, \pm 1, \pm 2, \pm 3$ $(L = 0 \nrightarrow 0)$	If $\Delta S = \pm 1$ $\Delta L = 0, \pm 1$ $(L = 0 \nrightarrow 0)$	If $\Delta S = \pm 1$ $\Delta L = 0, \pm 1,$ $\pm 2, \pm 3 \pm 4$ $(L = 0 \nrightarrow 0{,}1)$	If $\Delta S = \pm 1$ $\Delta L = 0, \pm 1,$ ± 2 $(L = 0 \nrightarrow 0)$

Figure 6: Radiative Transition's selection rules (table recreated from Wikipedia)

where $\pi = (-1)^l$ is the parity of each state with angular momentum l and the symbol $\nleftrightarrow$ is used to indicate a forbidden transition. In the hyperfine structure, the total angular momentum of the atom is $F = I + J$, where I is the nuclear spin angular momentum. Since, $F = I + J$ has the same mathematical form as J= $L + S$, it obeys a set of selection rules similar to the table above.

The above treatment gives the basic theoretical backdrop of the main transition studied in this thesis, namely the $5P_{3/2} \rightarrow 5P_{1/2}$ transition of atomic iodine, predominantly an M1 transition, which, however, contains weak E2 contributions, observed for the first time in this work, to the best of our knowledge.

Chapter 3: Absorptivity and absorption cross section

3.1 Refractive index of atomic vapor

We use a semi-classical model to describe a two-level atom, that of a single electron bound by a harmonic force to the nucleus, acted upon by the electric field of an incident light field.

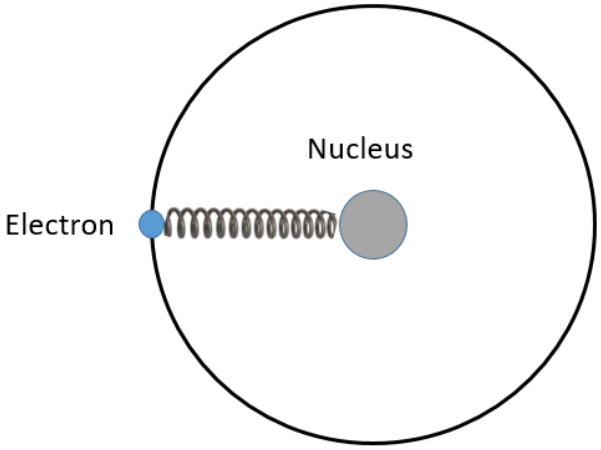

Figure 7: Semi-classical model of an atom.

In this case, the equation of motion for the electron around the atom is given by:

$$m_e[\ddot{x} + \gamma\dot{x} + \omega_0^2 x] = -eE(x,t) \tag{3.1}$$

where x is the position of the electron along the electric field direction, m_e is the mass of electron (assuming that the nucleus of the atom is much more massive compared to the electron), e is the electron charge, γ is the damping term, ω_0 is the resonant frequency. In the case of an electric field varying in time as $Ee^{i\omega t}$, then the dipole moment of a single atom is

$$p = -ex = \frac{e^2}{m_e}(\omega_0^2 - \omega^2 - i\omega\gamma)^{-1}E = \varepsilon_0\chi_e E \tag{3.2}$$

where χ_e is the electric susceptibility. If there are *N* atoms per unit volume, then the dielectric constant is given by:

$$\frac{\varepsilon(\omega)}{\varepsilon_0} = 1 + 4\pi\chi_e = 1 + \frac{4\pi N f e^2}{m_e(\omega_0^2 - \omega^2 - i\omega\gamma)} \tag{3.3}$$

where *f* is the oscillator strength of the transition.

The index of refraction is defined as $n = \frac{c}{u} = \sqrt{\frac{\varepsilon\mu}{\varepsilon_0\mu_0}}$. Assuming that $\frac{\mu}{\mu_0} \approx 1$, combined with equation *(3.3)*, the refractive index can be rewritten as

$$n = \sqrt{\frac{\varepsilon}{\varepsilon_0}} = n' + in'' \Longrightarrow$$

$$n(\omega) = 1 - \frac{\frac{\pi N f e^2 \Delta\omega}{\omega_0 m_e}}{\Delta\omega^2 + \frac{\gamma^2}{4}} + \frac{\frac{i\pi N f \gamma e^2}{2\omega_0 m_e}}{\Delta\omega^2 + \frac{\gamma^2}{4}} \tag{3.4}$$

Hence,

$$Re(n) = n' \approx 1 - \frac{\pi \Delta\omega N f e^2 / m_e \omega_0}{\Delta\omega^2 + \Gamma^2} \tag{3.5}$$

$$Im(n) = n'' \approx \frac{\pi N \Gamma f e^2 / m_e \omega_0}{\Delta\omega^2 + \Gamma^2} \tag{3.6}$$

where $\Delta\omega = \omega - \omega_0$ and $\Gamma = \gamma/2$ [8]. Plots of the imaginary and real parts of n as a function of frequency ω are shown in Figure 8. Note that the real part of the refractive index in the vicinity of the resonance frequency, rises rapidly at first, then drops below unity, and eventually makes its way back up toward unity. This behavior near resonance is called anomalous dispersion. Far from resonance the n' increases with the increasing of frequency, which is called normal dispersion. The imaginary part of the refractive index, n'', near the resonance increases sharply to a maximum then drops as the frequency exceeds the resonance frequency.

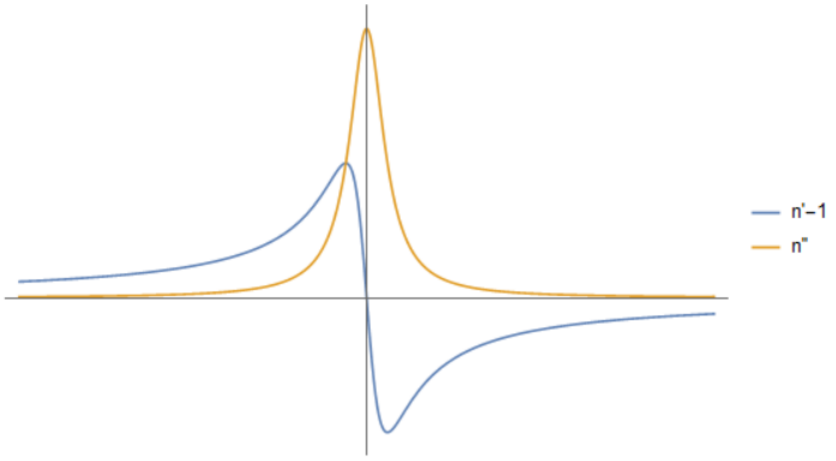

Figure 8: Dispersion and Absorption of EM in a vapor

The frequency dependence of equation *(3.6)* is Lorentzian. So, the dispersive and the absorptive parts of the lineshape function can take the form:

$$\mathcal{L}'(\Delta\omega) = \frac{1}{\pi}\frac{\Delta\omega}{\Delta\omega^2 + \Gamma^2} \tag{3.7}$$

$$\mathcal{L}''(\Delta\omega) = \frac{1}{\pi}\frac{\Gamma^2}{\Delta\omega^2 + \Gamma^2} \tag{3.8}$$

Hence, equation *(3.4)* can be rewritten as

$$n = n' + in'' = 1 + \frac{\pi\mu_0 e^2}{4m_e\omega_0} Nf\mathcal{L}(\Delta\omega) \tag{3.9}$$

where $\mathcal{L} = \mathcal{L}' + i\mathcal{L}''$.[3]

3.2 Refractive index including Doppler broadening

To obtain a better agreement between experiment and theory we must include the effect of *Doppler broadening*, since, in a thermal vapor, the Doppler effect due to the thermal motion of the atoms, leads to the dominant spectral broadening mechanism, and can not be neglected.

The frequency ω must be substituted by its Doppler-shifted value, $\omega - \boldsymbol{k} \cdot \boldsymbol{v}$, where k is the wavenumber and v the atomic velocity. The final step is to integrate the Lorentzian broadenings of the individual atoms over the Gaussian distribution for the atomic velocities (Maxwell-Boltzmann distribution), yielding the so-called *Voigt* profile. The Voigt profile can be expressed through the *Faddeeva function*, $w(z)$, which is a scaled complex complementary error function defined as:

$$w(z) = e^{-z^2} Erfc(-iz) = w'(x,y) + iw''(x,y) \tag{3.10}$$

where $z = x + iy$. For an atom with mass M and for a resonance frequency ω_0, the Doppler half-width at 1/e is:

$$\Delta\omega_D = \omega_0 \sqrt{\frac{2k_B T}{Mc^2}} \tag{3.11}$$

and the absorptive and dispersive parts of the lineshape are related to the w' and w'', respectively, via:

$$\mathcal{L}''(\Delta\omega) \rightarrow V''(\Delta\omega) = \frac{w'\left(\frac{\Delta\omega}{\Delta\omega_D}, \frac{\Gamma}{\Delta\omega_D}\right)}{\sqrt{\pi}\Delta\omega_D} \tag{3.12}$$

$$\mathcal{L}'(\Delta\omega) \rightarrow V'(\Delta\omega) = \frac{w''\left(\frac{\Delta\omega}{\Delta\omega_D}, \frac{\Gamma}{\Delta\omega_D}\right)}{\sqrt{\pi}\Delta\omega_D} \tag{3.13}$$

Hence,

$$n = n' + in'' = 1 + \frac{\pi\mu_0 e^2}{4m_e\omega_0} NfV(\Delta\omega) \tag{3.14}$$

where $V = V' + iV''$.

From equations *(A4)* and *(A5)*, where we define the oscillator strength for a *magnetic dipole interaction*, we can rewrite equation *(3.14)* as:

$$n = 1 + \frac{\pi\mu_0}{3} \frac{N}{2\hbar} \frac{|M1|^2}{(2J_a + 1)} V(\Delta\omega) \tag{3.15}$$

Assuming a non-zero nuclear spin, *I*, we must take into account the hyperfine structure. Using

$$\langle F_a|T^{(k)}|F_b\rangle = (-1)^{I+k+J_a+F_b}\sqrt{(2F_a+1)(2F_b+1)}\begin{Bmatrix} J_a & k & J_b \\ F_b & I & F_a \end{Bmatrix}\langle J_a|T^{(k)}|J_b\rangle \tag{3.16}$$

Where *k* is the tensor rank of the operator *T*, and the fact that the population of the ground state F_a is:

$$N(F_a) = \frac{2F_a+1}{(2J_a+1)(2I+1)}N \tag{3.17}$$

then from equation *(3.14)* and Appendix A, we get:

$$n = 1 + n_0 \sum_{F_a,F_b} C_{F_a,F_b} V_{F_a,F_b}(\Delta\omega) \tag{3.18}$$

where

$$n_0 = \frac{\pi\mu_0}{3}\frac{N}{2\hbar}\frac{|M1|^2}{(2J_a+1)} \tag{3.19}$$

$$C_{F_a,F_b} = \frac{(2F_a+1)(2F_b+1)}{(2I+1)}\begin{Bmatrix} J_a & k & J_b \\ F_b & I & F_a \end{Bmatrix}^2 \tag{3.20}$$

Where again $M1 = \frac{e}{2m_e c}\langle J_a|\hat{\boldsymbol{L}} + 2\hat{\boldsymbol{S}}|J_b\rangle$.[3] For the particular transition under study in atomic iodine, preliminary calculations yield $M1 = 1.15\ \mu_B$.

3.3 Including the electric quadrupole interaction

In the previous section we assumed a pure magnetic dipole interaction. However, given high enough angular momenta, the selection rules allow for the existence of higher order multipole interactions, as well, such as an electric quadrupole interaction. The quadrupole operator for the projection q is:

$$E2 = -\frac{q\omega}{4\sqrt{3}}Q_q^{E2} \tag{3.21}$$

where Q_q^{E2} is given by equation *(2.21)*. In order to find the refractive index, we must include the quadrupole interaction to the reduced matrix element

$$\frac{M1}{3} \rightarrow \frac{e}{2m_e c}\left\langle J_a\left|\boldsymbol{M_q} - \frac{q\omega}{4\sqrt{3}}\boldsymbol{Q_q^{E2}}\right|J_b\right\rangle \tag{3.22}$$

Then, we introduce the electric quadrupole to magnetic dipole ratio parameter, χ:

$$\chi = \frac{\omega}{4\sqrt{3}}\frac{\langle J_a|\boldsymbol{Q_q^{E2}}|J_b\rangle}{\langle J_a|\boldsymbol{M_q}|J_b\rangle} \tag{3.23}$$

Hence, the refractive index *(3.18)* can be rewritten as:

$$n = 1 + n_0 \sum_{F_a,F_b} C'_{F_a,F_b} V_{F_a,F_b}(\Delta\omega) \tag{3.24}$$

Where n_0 is the same quantity as equation *(3.19)* and

$$C'_{F_a,F_b} = \frac{(2F_a+1)(2F_b+1)}{(2I+1)}\left(\begin{Bmatrix} J_a & 1 & J_b \\ F_b & I & F_a \end{Bmatrix}^2 + \frac{3\chi^2}{5}\begin{Bmatrix} J_a & 2 & J_b \\ F_b & I & F_a \end{Bmatrix}^2\right) \quad [4] \qquad (3.25)$$

3.4 Beer-Lambert law and the absorption coefficient

Absorption of light in a medium is usually defined as the fraction of the power dissipated per unit length of the medium. If a beam is propagating in the $+z$ direction and the intensity at position z is $I(z)$, then the decrease of intensity across an incremental slice of thickness dz is given by:

$$dI = (-a)dz \times I(z) \qquad (3.26)$$

By integrating, we obtain Beer-Lambert law,

$$I(z) = I(0)e^{-az} \qquad (3.27)$$

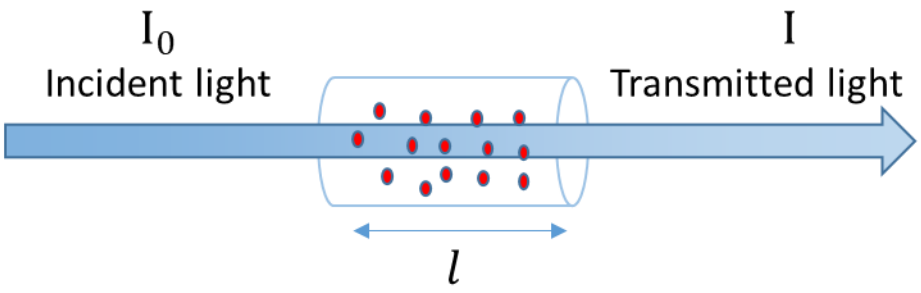

Figure 9: Beer- Lambert law.

The coefficient a is called absorption coefficient. We can generalize the wave-vector by using equation *(3.9)* as:

$$k = n\frac{\omega}{c} = (n' + in'')\frac{\omega}{c} \qquad (3.28)$$

Substituting that in our plane solutions

$$E_y(z,t) = Re\{A_1 e^{i(\omega t - kz)}\} + Re\{A_2 e^{i(\omega t + kz)}\} \qquad (3.29)$$

$$E_y(z,t) = Re\left\{A_1 e^{i\left(\omega t - (n'+in'')\frac{\omega}{c}z\right)}\right\} + Re\left\{A_2 e^{i\left(\omega t + (n'+in'')\frac{\omega}{c}z\right)}\right\}$$

$$E_y = Re\left\{A_1 e^{n''\frac{\omega}{c}z} e^{i\left(\omega t - n'\frac{\omega}{c}z\right)}\right\} + Re\left\{A_2 e^{-n''\frac{\omega}{c}z} e^{i\left(\omega t + n'\frac{\omega}{c}z\right)}\right\} \qquad (3.30)$$

$$E_y = A_1 e^{n''\frac{\omega}{c}z}\cos(\omega t - n'\frac{\omega}{c}z) + A_2 e^{-n''\frac{\omega}{c}z}\cos(\omega t + n'\frac{\omega}{c}z) \qquad (3.31)$$

The intensity is proportional to the square of the magnitude of the electric field. Taking the second term only, for the sake of simplicity, we can say that if the electric field is decreasing

[4] See Appendix A for the analytic derivation.

by $e^{-n''\frac{\omega}{c}z}$, then the intensity of the wave is decreasing proportionally to $\left(e^{-n''\frac{\omega}{c}z}\right)^2 = e^{-2n''\frac{\omega}{c}z}$.

Comparing this to Beer's law, we obtain the relationship between the absorption coefficient a and the imaginary part of the refractive index n'' [9]:

$$a = 2n''\frac{\omega}{c} \tag{3.32}$$

Hence, the transmission of light power through a vapor is governed by the Beer' law:

$$T(\omega) = \frac{I(\omega)}{I_0} = e^{-2\omega n''(\omega)l/c} = e^{-N\sigma(\omega)l} \tag{3.33}$$

where σ is the absorption cross section, l the length of the interaction area. From the previous discussion in section 3.2 it is obvious that the absorption cross section is given by:

$$\sigma(\Delta\omega) = \sigma_0 \sum_{F_a,F_b} C_{F_a,F_b} V''_{F_a,F_b}(\Delta\omega) \tag{3.34}$$

Where C_{F_a,F_b} is given by equation *(3.20) or (3.25)* , V''_{F_a,F_b} from equation *(3.12)* and, σ_0, the integrated absorption cross section, by [3]

$$\sigma_0 = \frac{\pi\mu_0\omega_0}{\hbar c}\frac{1}{2J_a+1}\frac{M1^2}{3} \tag{3.35}$$

Chapter 4: Faraday rotation

4.1 The Faraday Effect

In 1845, Michael Faraday discovered the first physical phenomenon linking light and magnetism. When plane polarized light propagates through a length l in certain magneto-optic mediums, with a magnetic field applied along the propagation direction making the medium optically active, its plane of polarization is rotated by an angle:

$$\varphi = V \int_0^l Bdl = VlB \tag{4.1}$$

where φ is the angle of rotation, V the Verdet coefficient, B the magnetic intensity, and l the length of the medium. Becquerel derived a classical expression for the Verdet constant,

$$V = \frac{\omega(n_+ - n_-)}{2cB} \tag{4.2}$$

Thus, the angle φ is given by:

$$\varphi = \frac{\omega l}{2c}(n_+ - n_-) \tag{4.3}$$

where n_+ and n_- are the refractive indices for the right- and left-circularly polarized components of light, respectively.

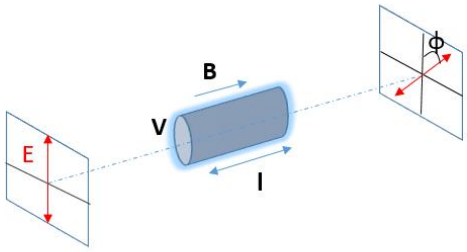

Figure 10: Faraday rotation through a transparent dielectric.

The Faraday phenomenon also appears near atomic and molecular resonances in the presence of an external magnetic field, due to the Zeeman effect, which affects the $n_\pm$ refractive indices. We consider an atomic vapor subject to a constant magnetic field B_z applied along the direction of propagation of the light. We assume that B_z is sufficiently weak for the Zeeman splittings of the hyperfine levels to be small compared with the intervals between adjacent hyperfine levels. Application of the field B_z affects the refractive index in two ways: through changes in the energies of the sublevels and through mixing of the states.

4.2 Symmetric part of Faraday rotation

Initially we consider only first order corrections to the system energy levels due to the magnetic field. The resonant frequency of the $|a\rangle \rightarrow |b\rangle$ transition becomes:

$$\omega_{ba} = \omega_0(F_b, F_a) - \frac{B_z}{\hbar}(\langle b|\mu_z|b\rangle - \langle a|\mu_z|a\rangle) \tag{4.4}$$

Where we use $|a\rangle$ to represent the ket $|J_a I F_a M_a\rangle$ and a, b labels, respectively, quantities referring to the ground and excited levels. The refractive index in the absence of the magnetic field is given by *(3.24)*.

Now, we must calculate the change in n_q, $q = \pm 1$ for right/left circularly polarized light, which is given by,

$$\begin{aligned} \delta n_q &= \frac{dn}{d\omega_{FF'}}\delta\omega_{FF'} \\ &= -\frac{\pi\mu_0 B_Z}{2\hbar^2}\sum_{\substack{F,F' \\ M,M'}}\frac{N(F_i)}{g_1}\left\langle F_a m_a\left|\mu_q^{(1)} - \frac{q\omega}{4\sqrt{3}}Q_q^{(2)}\right|F_b m_b\right\rangle^2 \\ &\times\left(\langle F_b|\mu_z|F_b\rangle - \langle F_a|\mu_z|F_a\rangle\right)V^*(\omega-\omega_{ba}) \end{aligned} \tag{4.5}$$

Where

$$V^*(\omega-\omega_{ba}) = \frac{\partial V'(\omega-\omega_{ba})}{\partial\omega_{ba}} = -\frac{1}{\Delta\omega_D}\frac{\partial V'(\omega-\omega_{ba})}{\partial\left(\frac{\omega-\omega_{ba}}{\Delta\omega_D}\right)} \tag{4.6}$$

Performing the summations over the *M* states results in the expression for the symmetric part of the Faraday angle:

$$\varphi_s = \frac{\mu_0\pi B_z}{2\hbar^2}\frac{\omega l}{c}\frac{N(F_a)M1^2}{2F_a+1}(U_{11}+2U_{12}x+U_{22}x^2)V^*(\omega-\omega_{ba}) \tag{4.7}$$

Where the expression for U_{xy} is given by

$$\begin{aligned} U_{xy} = (-1)^{1+x}&\frac{(2F_x+1)(2F_y+1)}{[x(x+1)(2y+1)]^{\frac{1}{2}}}\begin{Bmatrix} j_y & x & j_x \\ F_x & I & F_y\end{Bmatrix}\begin{Bmatrix} j_y & y & j_x \\ F_x & I & F_y\end{Bmatrix} \\ &\times\left[\left((-1)^{j_y-F_x+I}(2F_y+1)\begin{Bmatrix} j_y & 1 & j_y \\ F_y & I & F_y\end{Bmatrix}\begin{Bmatrix} x & 1 & y \\ F_y & F & F_y\end{Bmatrix}\right)\right. \\ &\left.+\text{ same terms with } (-1)^{x+y}\begin{pmatrix} j_y & \leftrightarrow & j_x \\ F_y & \leftrightarrow & F_x\end{pmatrix}\right] \end{aligned} \tag{4.8}$$

And the allowed combinations of (*x*, *y*) are (1, 1), (2, 2) and (1, 2), *x* takes the value 1 for the magnetic dipole term and 2 for the electric quadrupole term.

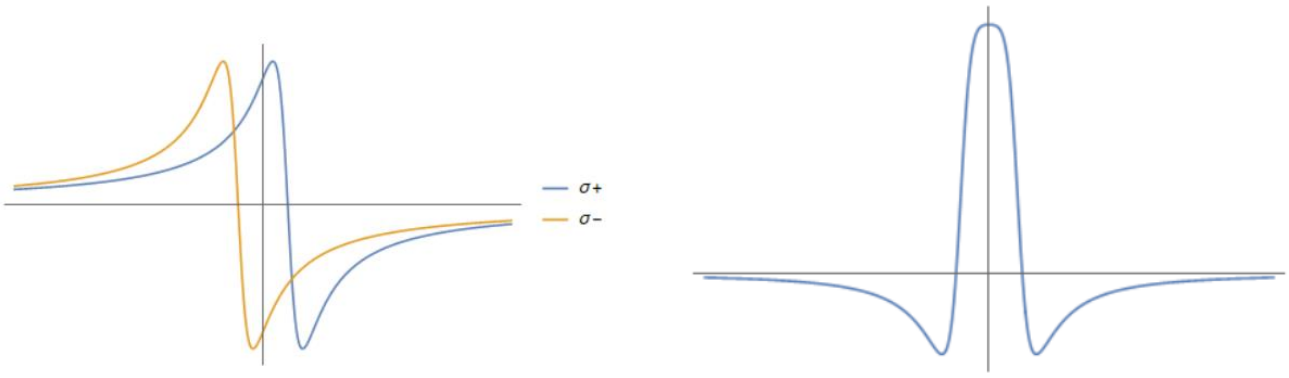

Figure 11: a) Refractive index line shapes for left (σ+) and right (σ-) circularly polarized light near an atomic resonance in the case of Zeeman splitting and b) the symmetric part of faraday rotation line shape.

4.3 Antisymmetric part of Faraday rotation

Another effect of the magnetic field is that it mixes states of the same M but with different F so that a state $|FM\rangle$ becomes

$$|F_a M\rangle \rightarrow |F_a M\rangle - \sum_{F_a \neq F_k} \frac{\langle F_k M|\mu_z|F_b M\rangle}{\hbar\omega_0(F_b, F_k)} |F_k M\rangle B_z \tag{4.9}$$

Hence, the consequent change in n_q is

$$\delta n_q = \frac{\mu_0 \pi B_z}{2\hbar} \sum_{\substack{F_a F_b \\ M_a M_b}} \frac{N(F_a)}{2F_a + 1}$$

$$\Bigg[\Bigg(\sum_{F_k \neq F_b} \frac{1}{\hbar\omega_0(F_b, F_k)} \left(\langle F_k M_b|\mu_z|F_b M_b\rangle\langle F_b M_b|\mu_q|F_a M_a\rangle\langle F_a M_a|\mu_{-q}|F_k M_b\rangle\right)$$

$$+ \langle F_b M_b|\mu_z|F_k M_b\rangle\langle F_k M_b|\mu_q|F_a M_a\rangle\langle F_a M_a|\mu_{-q}|F_b M_b\rangle\Bigg)$$

$$+\Bigg(\sum_{F_l \neq F_a} \frac{1}{\hbar\omega_0(F_a, F_l)} \left(\langle F_a M_a|\mu_z|F_l M_a\rangle\langle F_l M_a|\mu_{-q}|F_b M_b\rangle\langle F_b M_b|\mu_q|F_a M_a\rangle\right)$$

$$+ \langle F_l M_a|\mu_z|F_a M_a\rangle\langle F_a M_a|\mu_{-q}|F_b M_b\rangle\langle F_b M_b|\mu_q|F_l M_a\rangle\Bigg)$$

$$+\left(\mu_q \rightarrow Q_q^{(2)}\right) + \left(\mu_{-q} \rightarrow Q_{-q}^{(2)}\right) + \left(\mu_{\pm q} \rightarrow \mp Q_{\pm q}^{(2)}\right)\Bigg] V'(\omega - \omega_{ba}) \tag{4.10}$$

Performing the summations over the M states results in the expression for the symmetric part of the Faraday angle

$$\varphi_a = \frac{\mu_0 \pi B_z}{\hbar^2} \frac{\omega l}{c} \frac{N(F_a) M 1^2}{2F_a + 1} (V_{11} + V_{12} x + V_{22} x^2) V'(\omega - \omega_{ba}) \tag{4.11}$$

Where the expression for V_{xy} is given by

$$V_{xy} = (-1)^x \frac{(2F_x+1)(2F_y+1)}{[x(x+1)(2y+1)]^{\frac{1}{2}}}$$
$$\times \left\{ \left[\sum_{F_k \neq F_y} (-1)^{j_y - F_x + I} (2F_y+1) \begin{Bmatrix} j_y & 1 & j_y \\ F_y & I & F_k \end{Bmatrix} \times \frac{\langle j_y | \mu^{(1)} | j_y \rangle}{\omega_0(F_y, F_k)} \right.$$
$$\times \left(\begin{Bmatrix} j_y & x & j_x \\ F_x & I & F_y \end{Bmatrix} \begin{Bmatrix} j_y & y & j_x \\ F_x & I & F_k \end{Bmatrix} \begin{Bmatrix} y & 1 & x \\ F_y & F_x & F_k \end{Bmatrix} \right.$$
$$\left. \left. + \begin{Bmatrix} j_y & y & j_x \\ F_x & I & F_y \end{Bmatrix} \begin{Bmatrix} j_y & x & j_x \\ F_x & I & F_k \end{Bmatrix} \begin{Bmatrix} x & 1 & y \\ F_y & F_x & F_k \end{Bmatrix} \right) \right]$$
$$\left. + \text{terms } (-1)^{x+y+1} \begin{bmatrix} j_y & \leftrightarrow & j_x \\ F_y & \leftrightarrow & F_x \\ F_k & \rightarrow & F_l \end{bmatrix} \right\} \tag{4.12}$$

And the allowed combinations of (x, y) are (1, 1), (2, 2) and (1, 2)

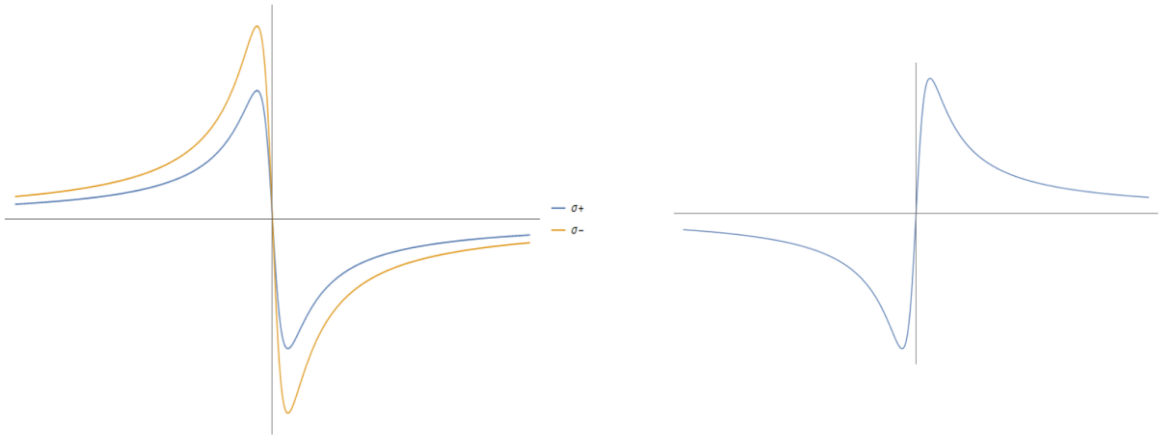

Figure 12: a) Refractive index line shapes for left (σ+) and right (σ-) circularly polarized light in the case of mixed states and b) the antisymmetric part of faraday rotation line shape.

Chapter 5: Atomic Iodine

5.1: Iodine (^{127}I)

Iodine, with $Z = 53$, is an atom with ground state configuration of $5p^5$. There are 37 known isotopes of iodine ($_{53}$I) from ^{108}I to ^{144}I; all undergo radioactive decay except ^{127}I, which is stable. Moreover, ^{127}I, as an odd-Z isotope, has non-zero nuclear spin, $I = \frac{5}{2}$, and therefore, nuclear spin–dependent effects can be measured.

The spin-orbit interaction is described by the LS-coupling, therefore, the two term symbols which arise are $^2P_{3/2}$for the ground state, and $^2P_{1/2}$ for the first excited state. Taking into account the hyperfine interaction we can draw the energy scheme of Figure 13. From the selection rules, Figure 6, we see that the electric dipole (E1) transition is forbidden. Hence, as per the selection rules, the lowest allowed multipole interactions are the magnetic dipole (M1) and electric quadrupole (E2). In Figure 13, blue lines indicate transitions that are both M1- and E2-allowed, while red lines indicate E2-specific ones.

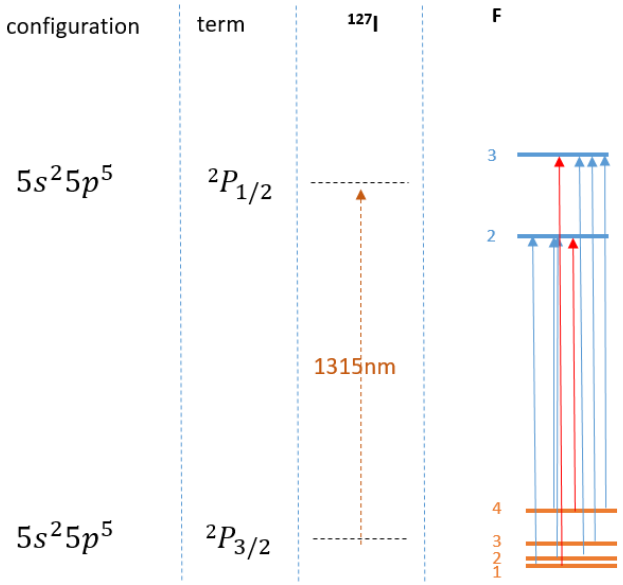

Figure 13: Energy level scheme for the $^2P_{3/2} \rightarrow {}^2P_{1/2}$ M1 (and E2) transition of atomic iodine at 1315nm. The blue arrows indicate the M1 (and weakly E2), and the red arrows the E2-exclusive hyperfine transitions.

5.2: Production of high density I ($^2P_{3/2}$) atoms

High iodine densities of $\sim 10^{16} cm^{-3}$ have been achieved in DC glow discharges or by using high-temperature ovens. Both of these methods lead to large spectral broadenings, in the first case pressure broadening (Lorentzian) and in the second case Doppler broadening (Gaussian). Desiring to keep broadening of the spectral lines to a minimum, we consider an alternative method for the creation of ground-state $^2P_{3/2}$ iodine atoms through *photodissociation* of I_2 molecules with an intense 532nm laser [10]:

$$I_2 \xrightarrow{h\nu} I(2P_{3/2}) + I(2P_{3/2}) \tag{5.1}$$

We assume that the population of excited-state I_2, and production of I_3 trimers is negligible. After production, iodine atoms recombine mainly via two processes:

$$\textit{three-body recombination: } I(2P_{3/2}) + I(2P_{3/2}) + I_2 \xrightarrow{k_r} 2I_2 \qquad (5.2)$$
$$\textit{trapping to container wall: } I \xrightarrow{k_w} I_{wall}$$

where k_r is the recombination rate, $k_r = 4.4 \times 10^{-30}\text{ml}^2\text{s}^{-1}$ at room temperature[11], and k_w is the rate at which atomic iodine sticks to the cell walls, which is on the order of kHz.

The rate equation governing the production rate of atomic iodine from photodissociating I_2 is given by:

$$\frac{d[I]}{dt} = \sigma\Phi[I_2] - k_r[I]^2[I_2] - k_w[I] \qquad (5.3)$$

where $[I]$ and $[I_2]$ are the atomic and molecular iodine densities, respectively, $\sigma = 2.4 \times 10^{-18}\text{cm}^2$ is the I_2 photodissociation cross section at 532 nm, $\Phi = \frac{1}{A}\frac{P}{hc/\lambda}$ the green laser photon flux, A the cell cross sectional area and P the power of the green laser.

The steady state solution of *(5.3)* is:

$$[I] = \frac{-k_w + \sqrt{k_w^2 + 4[I_2]^2 k_r \sigma\Phi}}{2[I_2]k_r} \qquad (5.4)$$

A flux $\Phi \approx 10^{20}$ photons $\text{cm}^{-2}\text{s}^{-1}$, gives a steady state iodine-atom density $[I] \approx 10^{16}\text{cm}^{-3}$. Finally, assuming a cell with a length of 1 m and a high-finesse optical cavity with 100 passes, gives an upper bound for the effective I-atom vapor *column density* of $10^{20}cm^{-2}$ [12].

5.3: Absorption and Faraday rotation Simulations

In the case of hyperfine interaction, the energy levels of the hyperfine states are given by:

$$E_F = E_j + \frac{K}{2}A + \frac{3K(K+1) - 4IJ(I+1)(J+1)}{8IJ(2I-1)(2J-1)}B \qquad (5.5)$$
$$K = F(F+1) - I(I+1) - J(J+1) \qquad (5.6)$$

where E_j is the energy of the fine structure level with quantum number J, A is the magnetic dipole hyperfine constant, and B is the electric quadrupole hyperfine constant [13]. In the case of iodine the hyperfine coupling constants, as determined by previous work in our lab, are:

Hyperfine coupling constants		
Total Angular Momentum J	*Magnetic dipole [Hz]*	*Electric quadrupole [Hz]*
Ground state $J = 3/2$	8.3274×10^8	1.0804×10^9
Excited state $J = 1/2$	6.6695×10^9	0

So, we can simulate the transmission spectrum of iodine be using equations *(3.33), (3.34), (3.35)* and *(3.25)*. We assume a number density $\sim 10^{16}\text{cm}^{-3}$, room temperature, $T = 300\text{K}$, and a cell length of 45 cm, to get a column density $\sim 4.5 \times 10^{17}\text{cm}^{-2}$. At room temperature the Doppler broadening is ~ 150 MHz. The reduced matrix element for the magnetic-dipole operator is, according to preliminary calculations, $M1 = \langle J_a | \mu^{(1)} | J_b \rangle = 1.15\mu_B$. Firstly, we

neglect the E2 transition ($\chi = 0$), and take the transmission and absorptivity (= − natural logarithm of transmission) spectra versus the frequency detuning from the nominal transition frequency (Figure 14).

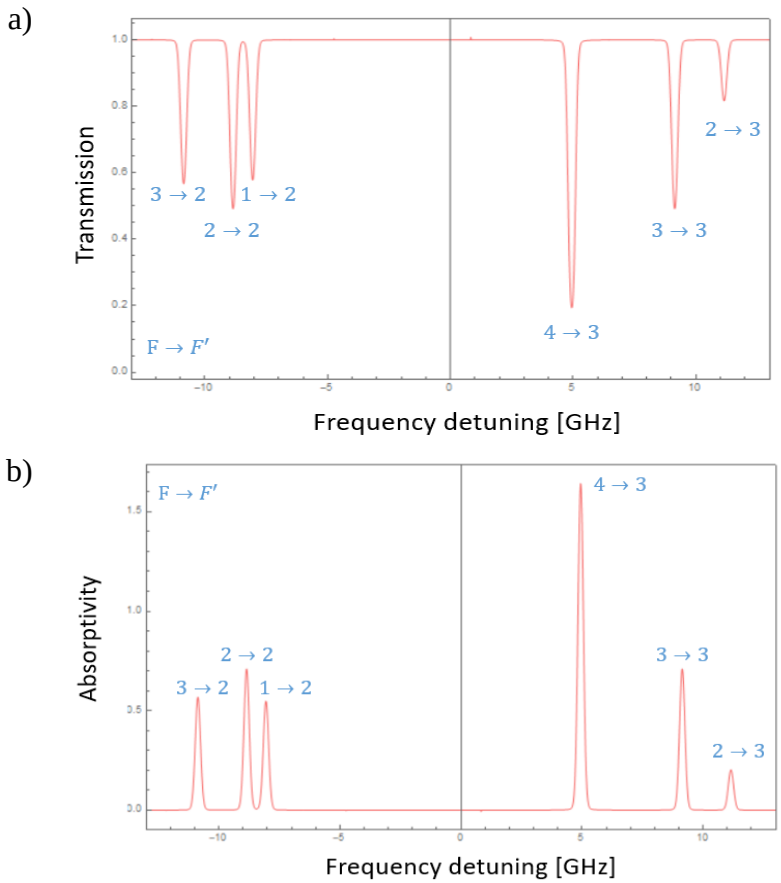

Figure 14: a) Transmission spectrum for the hyperfine magnetic dipole transitions and b) the absorptivity of the same transitions giving the corresponding optical depth.

Now, assuming a non-zero electric quadrupole to magnetic dipole ratio parameter χ, we get the hyperfine electric quadrupole transitions, which are shown in the following spectrum

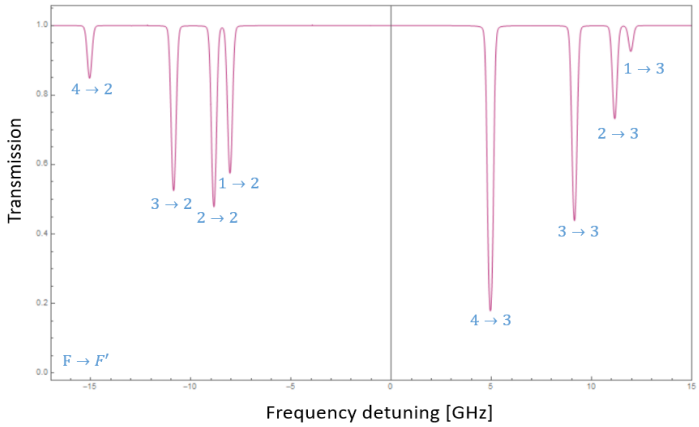

Figure 15: Transmission spectrum for the hyperfine magnetic dipole and electric quadrupole transitions for $\chi = 0.5$. The value of χ is chosen for clarity, and is significantly higher than the actual value.

Moving on to the Faraday rotation spectra, by taking into account the symmetric and antisymetric parts of the effect, and isolating one particular hyperfine transition (the magnetic dipole transition $F = 4$ to $F' = 3$), we can simulate our signals as follows. First, we only calculate the Faraday rotation spectrum versus the detuning in the absence of absorption, and then we include absorption, by multiplying with the transmission spectrum. The simulated signals are shown in Figure 16.

a)

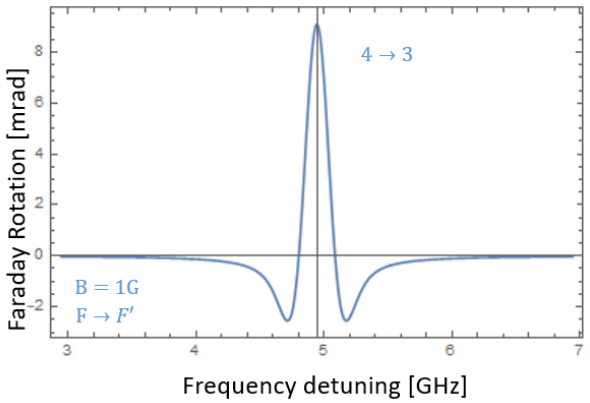

b)

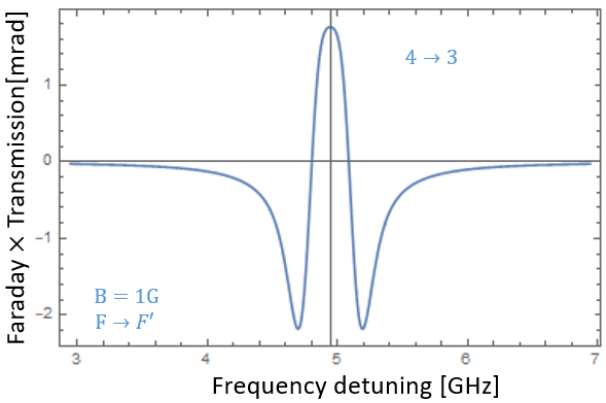

Figure 16:a) Faraday rotation for the magnetic dipole transition $F = 4$ to $F' = 3$ versus the detuning and b) the Faraday multiplied with the transmission spectra for a magnetic field $B = 1G$.

Chapter 6: Experimental Apparatus and results

6.1: Experimental Apparatus and Measurement Method

For all the measurements presented in this chapter, the same experimental setup was used. The basics of the experimental setup are shown in Figure 17. A bowtie, four-mirror cavity with round-trip cavity length $L = 2.6\text{m}$, $FSR = 115\text{MHz}$ and Finesse, $F \approx 240$ was used. The bowtie cavity consists of two concave mirrors with radius of curvature of 2m (one ATF mirror with specified reflectivity $R = 0.999\%$ at 1315nm, and one Layertec output coupler with reflectivity $R = 0.995\%$), and two plane mirrors (one ATF mirror with specified reflectivity $R = 0.999\%$ at 1315nm, and one Layertec coupler with reflectivity $R = 0.995\%$). The iodine cell was placed in one arm of the cavity. For the photodissociation of I_2 molecules to 2×I we used a green laser (HPL-532nm-cw, max power 50W) which was periodically chopped at a frequency of 20 Hz, so that we could also take background measurements, while for the IR spectroscopy of the M1 (and E2) transition, an IR laser (Toptica, DL pro) at 1315nm was employed.

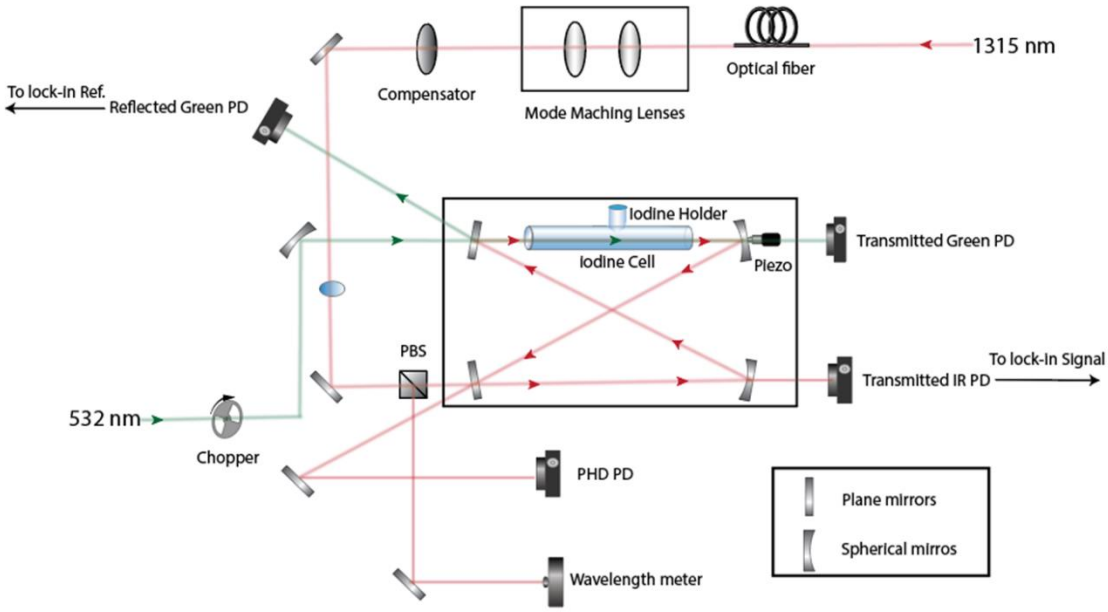

Figure 17: Schematic diagram of the experimental setup.

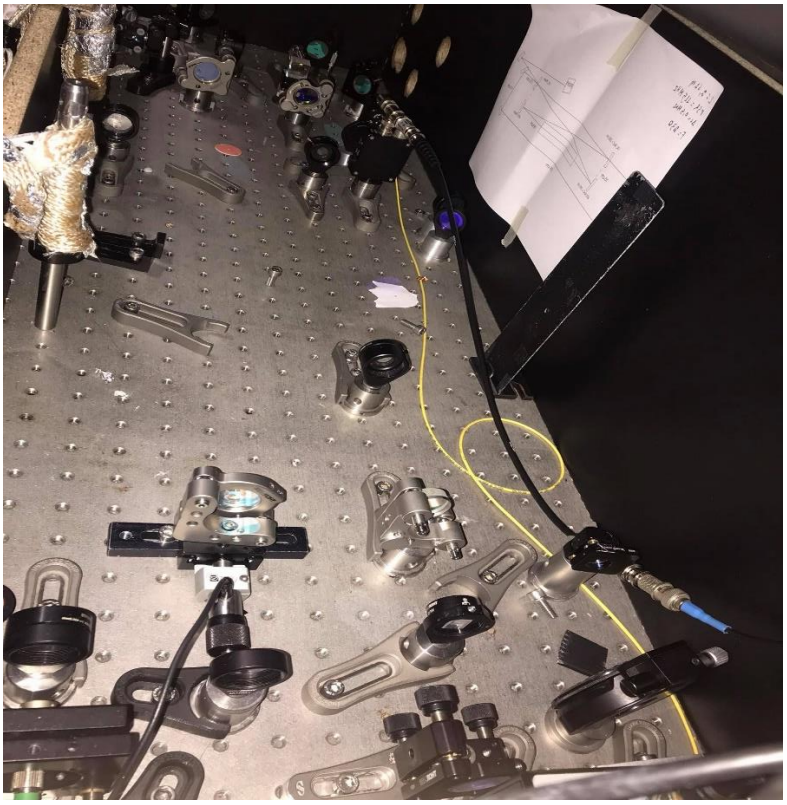

Figure 18: Experimental setup.

The IR laser beam was frequency-locked to a cavity resonance using the Toptica DigiLock 110 module and the Pound-Drever-Hall (PDH) technique (Figure 19). A piezoelectric transducer was placed on one mirror of the cavity in order to control the cavity length, and thus the resonant frequency of the cavity mode on which the laser was locked. By expanding or contracting the cavity via the piezo, while the laser remained locked to the same resonance, we could tune the laser frequency and scan over the iodine resonances. The laser frequency was measured with a wavelength meter (Bristol 671) and the reading was fed back to the piezo controller for further stabilization of the frequency, via a LabView PID *.vi* (Figure 20).

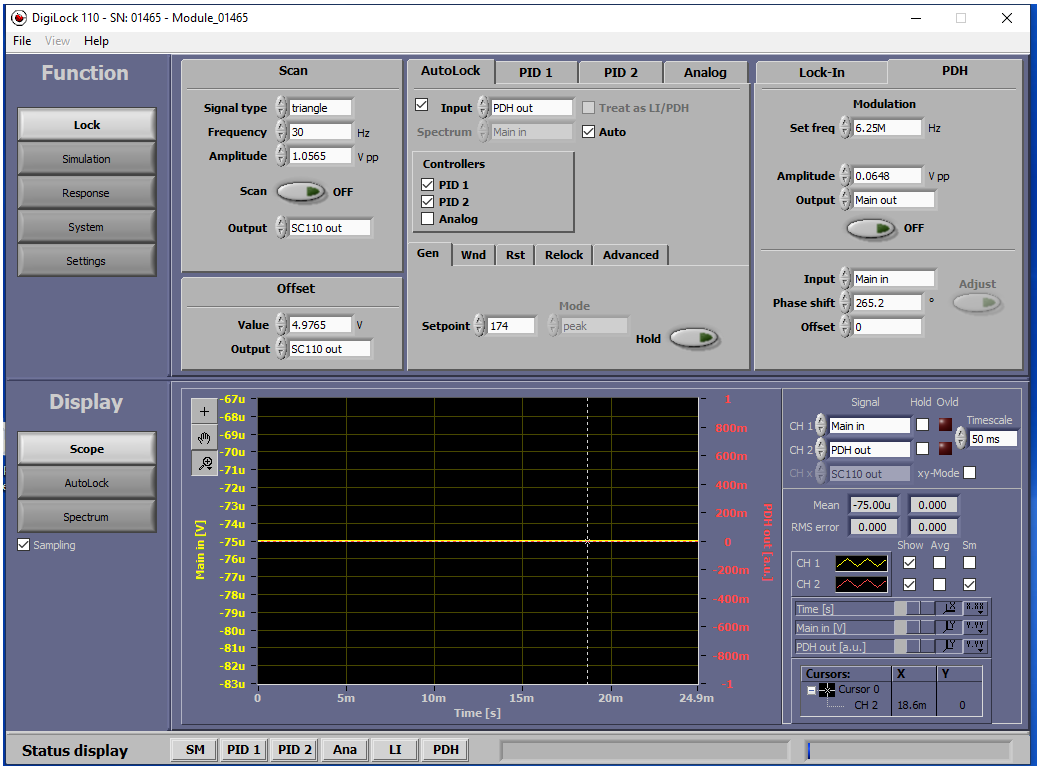

Figure 19: DigiLock Module

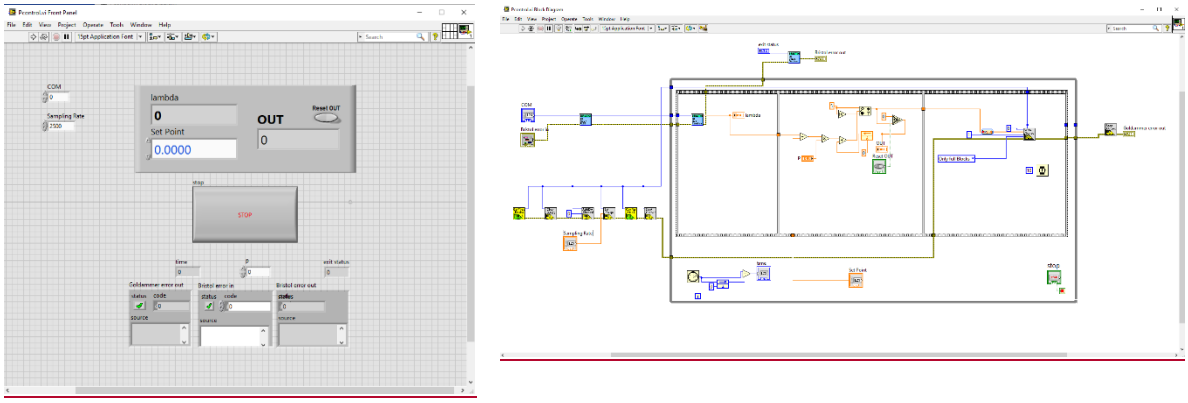

Figure 20: The PID labview program for the wavelength stabilaization.

Two photodiodes were used to record the signals, one for the reflected off the cavity part of the green laser and another for the IR. The two signals were then used as inputs for a lock-in amplifier (Ametec 7230 DSP Lock-in Amplifier), the – chopped – green signal as a frequency reference, and the IR as the spectroscopic input signal. The recorded signals and the output of the lock-in amplifier were displayed on an oscilloscope (Rohde & Schwarz RTO2034) which permitted signal averaging. An example of the acquired signals is shown in Figure 21.

a)

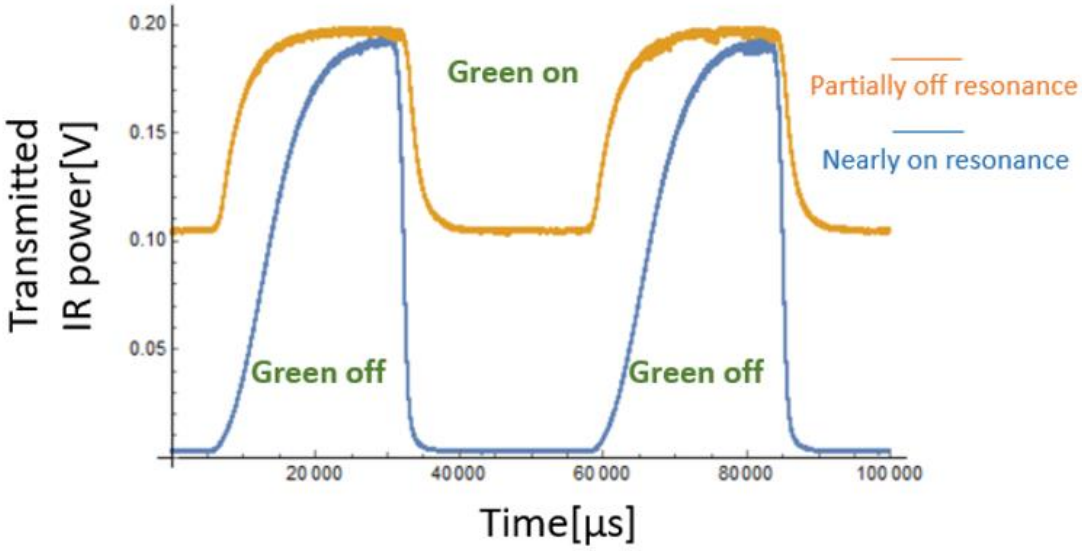

b)

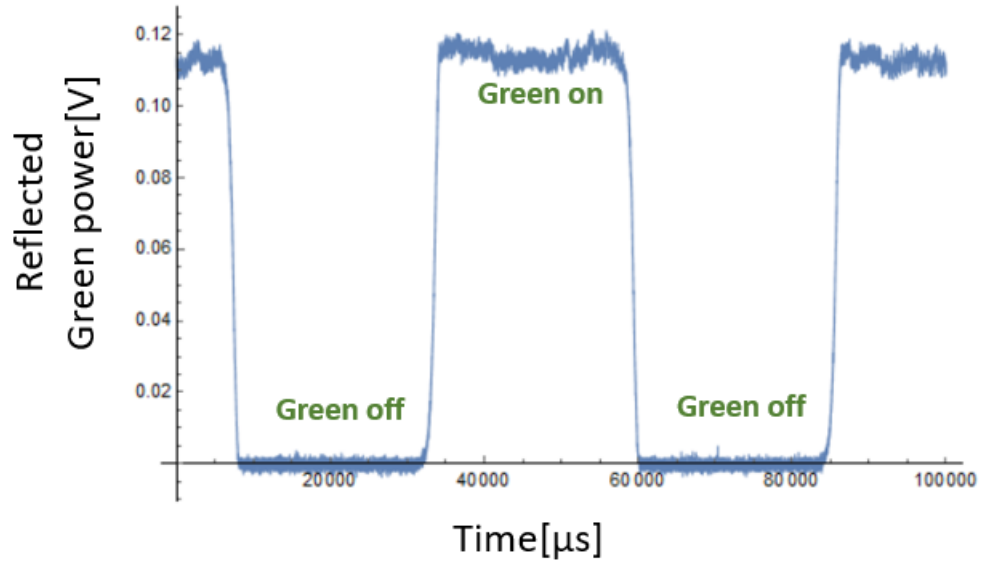

Figure 21:a) The recorded signals for different values of absorption. The green line is on resoncce while the orange and blue nearly of resonance.b) is the signal which is given to the lock-in as a reference in order to measure the amplitudes of the signals in figure a).

Notice that while the green light is abruptly turned on and off with the chopper, the rate at which the IR absorption changes in response is not equally abrupt. The reason for this behavior is that iodine photodissociates and recombines much more slowly than this chopping-on/off time. From analyzing these absorption responses, we can extract information about the photodissociation and recombination rates of iodine. Furthermore, the curves in Figure 21a interestingly seem to indicate that these rates are affected by the detuning of the IR laser from resonance (lest not forget that, due to the *cavity buildup* effect, the IR field inside the cavity can be quite intense). We defer conversation and an analysis of these observations to future work.

6.2: Experimental results

6.2.1: 20cm Iodine cell

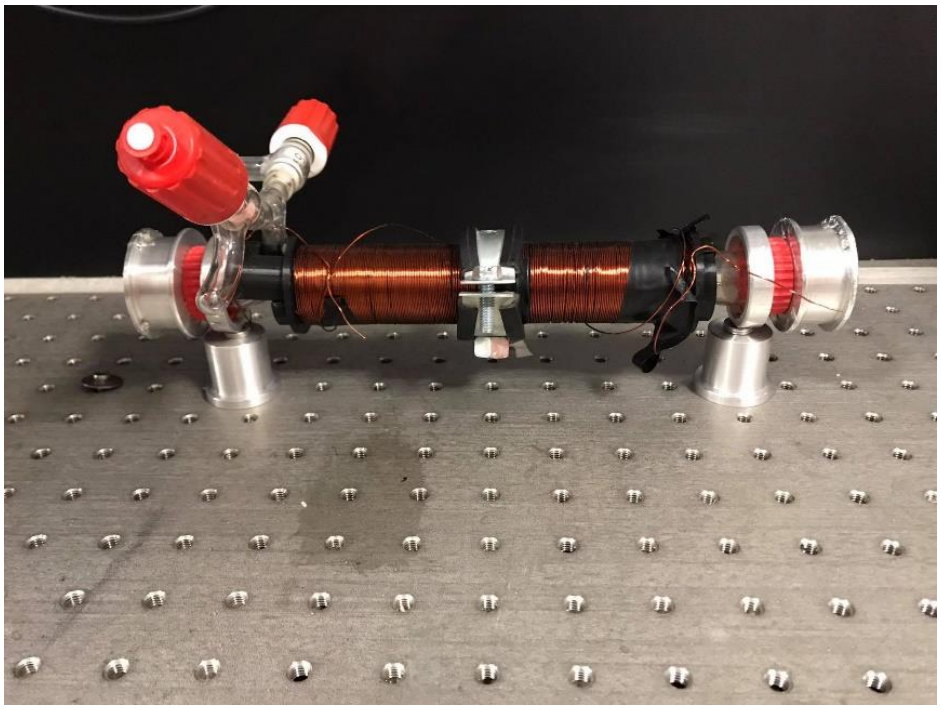

Figure 22:The 20cm iodine cell with diameter 2.54cm. The windows used were two ATF windows, AR coated at 1315nm with reflectivity R<0.01%.

Our initial measurements were performed using a 20 cm long, 1 inch diameter glass cell, fitted with two ATF AR-coated windows ($R < 0.01\%$).

A 5Watt green laser was used for the photodissociation, and we recorded transmission spectra of the atomic iodine over all hyperfine transitions with the method described in the previous section. In order to find the resonant frequencies and the transition linewidths, we fitted the data with Lorentzian functions as shown in Figure 23. The resonance frequencies and the FWHM are also shown in Figure 23. Notice that the spectra were closely fitted with Lorentzian functions, and the fits resulted in larger than expected linewidths. These were both results of pressure broadening, due to the cell not being adequately hermetically sealed, and our measurements taking long enough times for air to increase the pressure inside the cell.

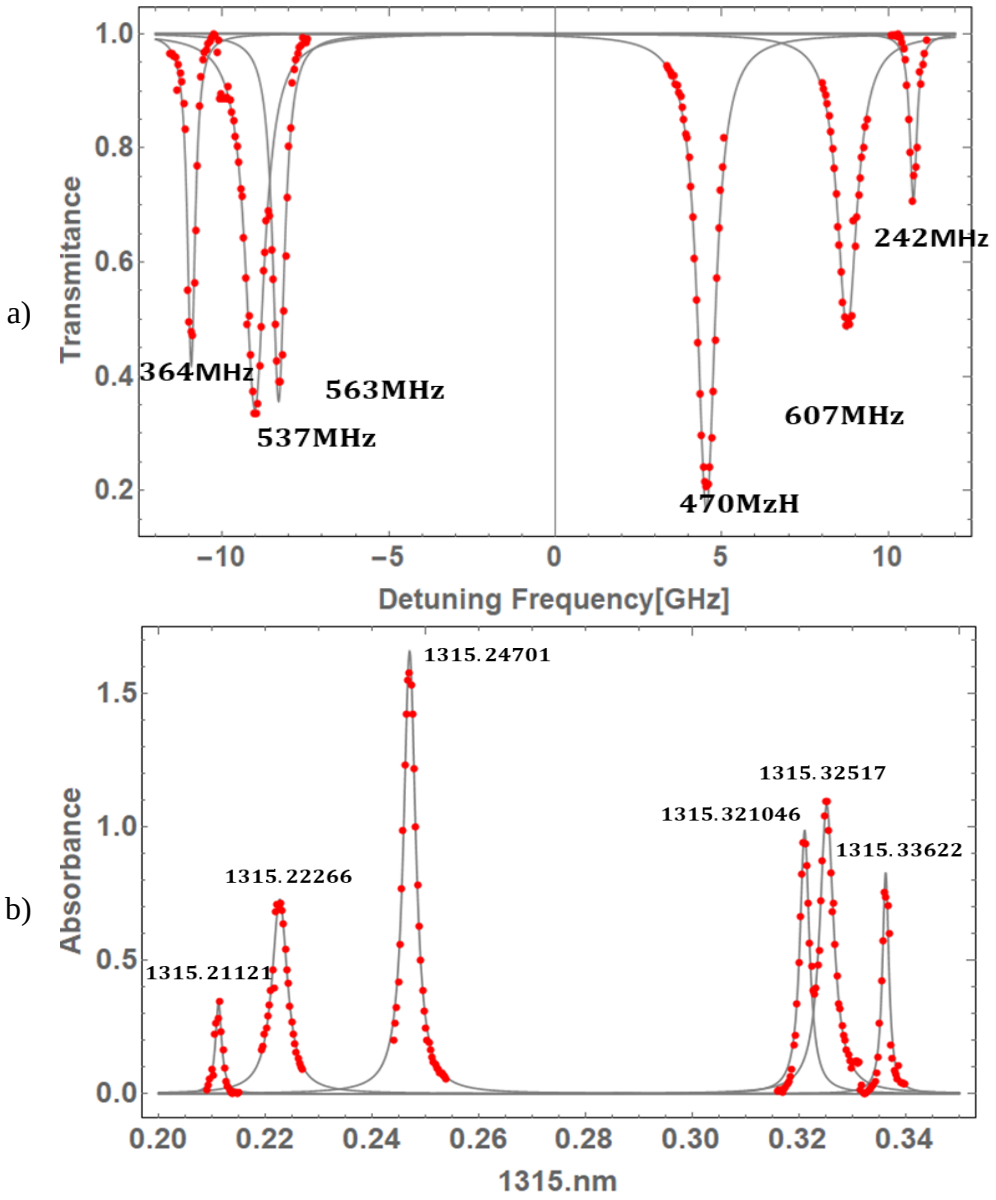

Figure 23:a) Transmittance of the M1 iodine transition as a function of the frequency detuning and b) corresponding absorbance spectrum as a function of wavelength this time, for reference, for 5Watt green power..

Next, we made a first attempt to measure the electric-quadrupole-exclusive transitions ($F = 1 \rightarrow F' = 3$ and $F = 4 \rightarrow F' = 2$) which are much weaker than the magnetic dipole transition, and we succeeded in measuring the $F = 4$ to $F' = 2$ transition as shown below. The absorption was found to be $\sim 0.5\%$. The weaker $F = 1 \rightarrow F' = 3$ E2 transition still remained out reach for our experimental conditions.

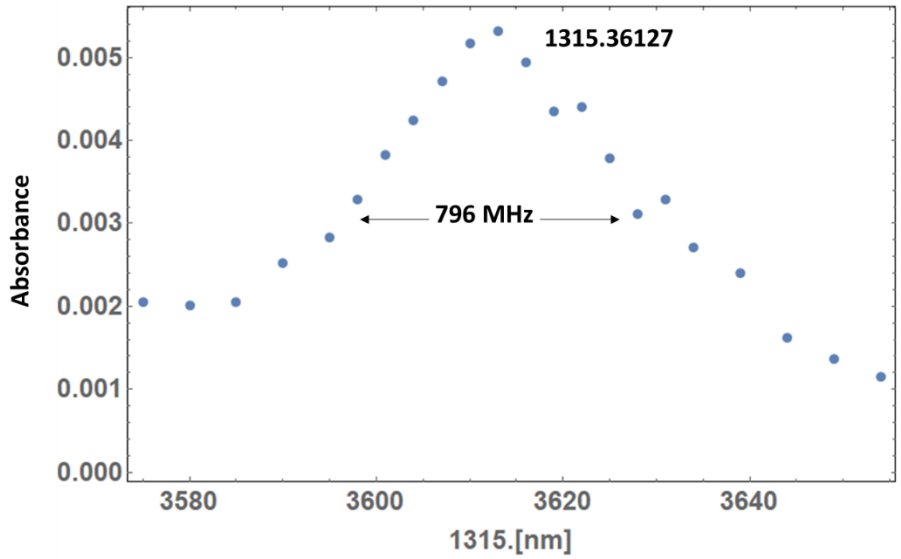

Figure 24: The $F = 4$ to $F' = 2$ quadrupole transition absorbance (in absorption-lengths) as a function of the wavelength for 5Watts of green power. The FWHM was estimated to be 796MHz.

To increase photodissociation, we substituded the 5W green laser with a 25Watt green laser in order to reach higher atomic iodine densities. We, again, measured IR spectra on the M1 transition as shown in Figure 25 and Figure 26.

a)

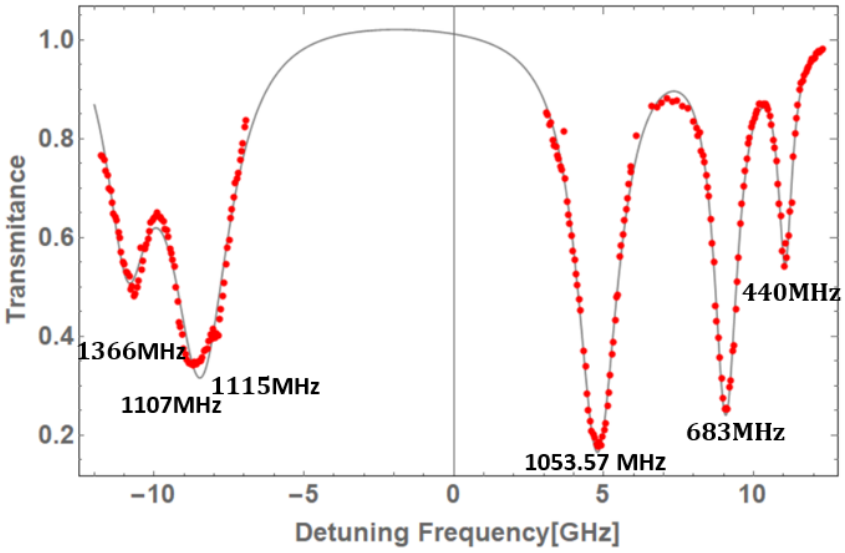

b)

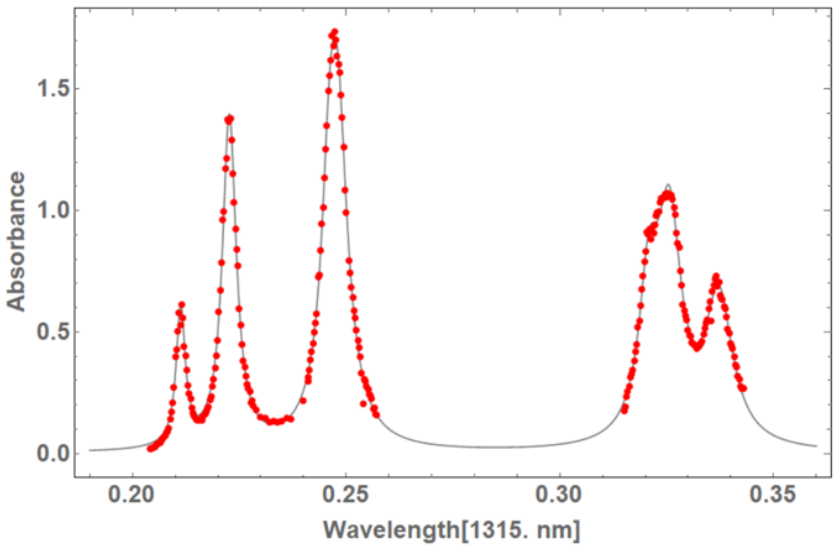

Figure 25:a) Transmittance of the M1 iodine transition as a function of the frequency detuning and b) corresponding absorbance spectrum as a function of wavelength this time, for reference, for 25Watt green power.

a)

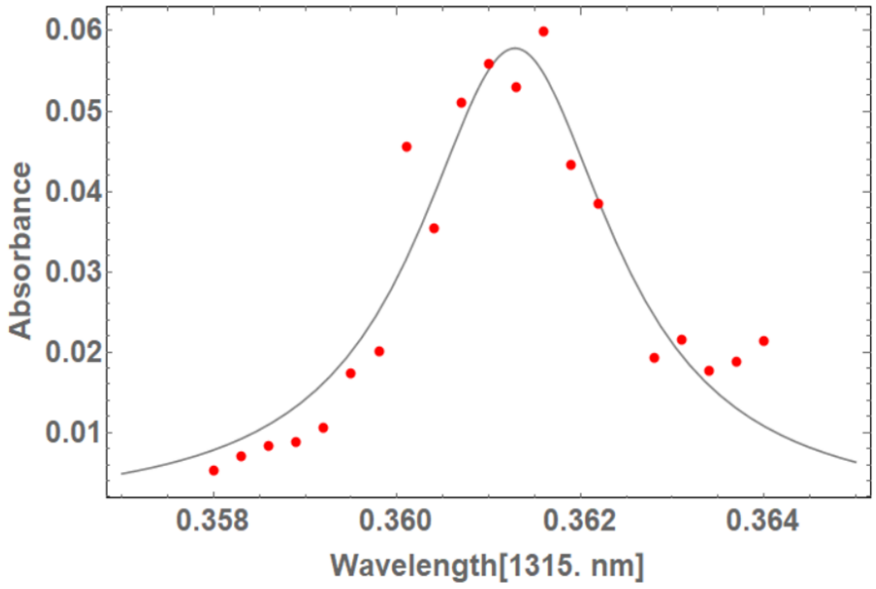

b)

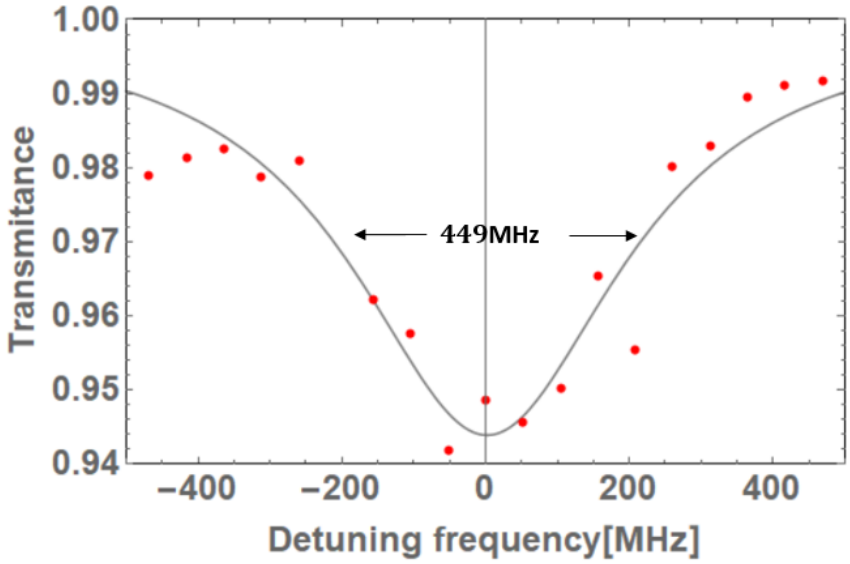

Figure 26: a) The $F = 4$ to $F' = 2$ quadrupole transition absorbance (in absorption lengths) as a function of the wavelength and b) the transmission as a function of the detuning for 25Watt green power. The FWHM was estimated to be 449MHz which is smaller than the 5Watt measurement because the cell was pumped before the measurement and the pressure broadening was smaller.

By using the 25 Watt laser we would expect to have higher absorptions compared to our previous attempts. From our results we do not observe significant changes in the absorption, but we do observe the detrimental effects of the inadequate sealing of our cell imprinted on the FWHM of the recorded lines. This is especially obvious in Figure 25, where the cell was initially pumped, and measurements were performed right-to-left: we see the FWHM, which should remain a constant throughout the measurements, increasing steadily due to the inflow of air and the increase of pressure in the cell.

Hence, in order to improve and stabilize our experimental conditions, we constructed a new sealed cell with length $l = 45\text{cm}$.

6.2.2: 45cm sealed Iodine cell

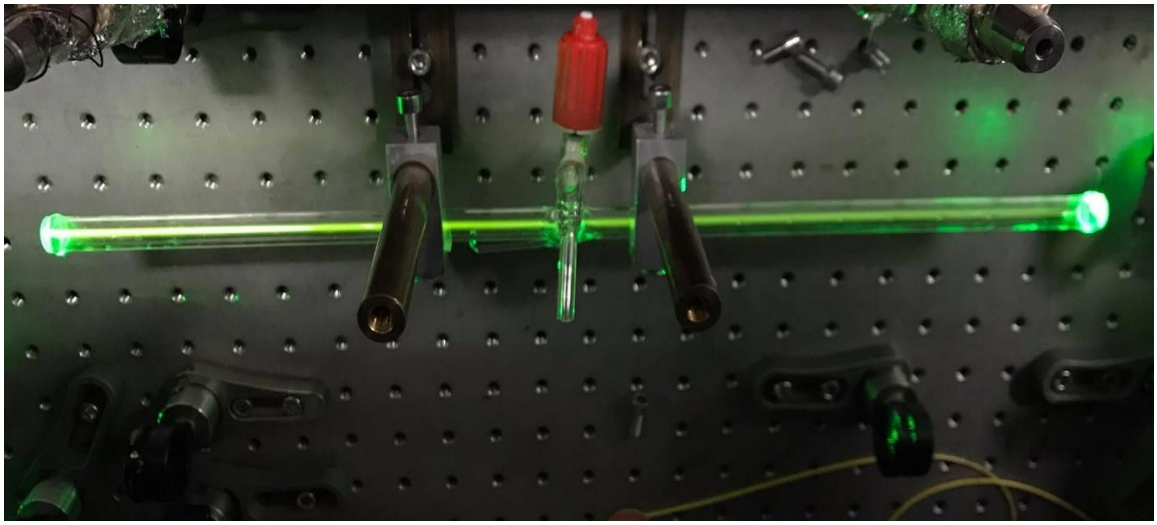

Figure 27: The 45cm sealed iodine cell with diameter 1.47cm. The windows which were used are two Eksma windows AR double coated at 1315nm with reflectivity R<0.04% and at 532nm with reflectivity R=0.02%.

The new cell was a 45 cm long, 8 mm internal diameter glass cell, with two ½-inch windows from EKSMA, AR-coated for both 1315 nm and 532 nm, epoxied on its edges. The performance of this cell in terms of maintaining vacuum after being pumped was vastly superior to our previous cell.

With the same experimental setup, the new sealed cell, and green laser power of $P \sim 20$ W we measured the iodine spectrum, as we see in Figure 28. A testament to the performance of the new cell, the data are now fitted with Gaussian functions, since, as expected, the main broadening mechanism is the Doppler Effect (room temperature Doppler broadening ≈ 150MHz, as opposed to a few MHz of Lorentzian pressure broadening due to collisions at a room temperature iodine pressure of ~0.2 mbar).

a)

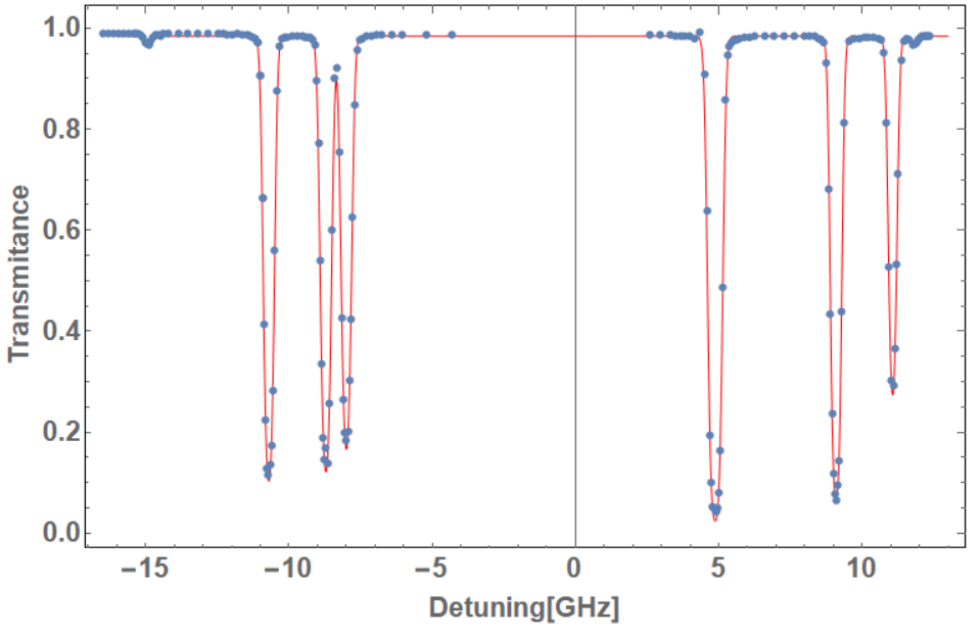

b)

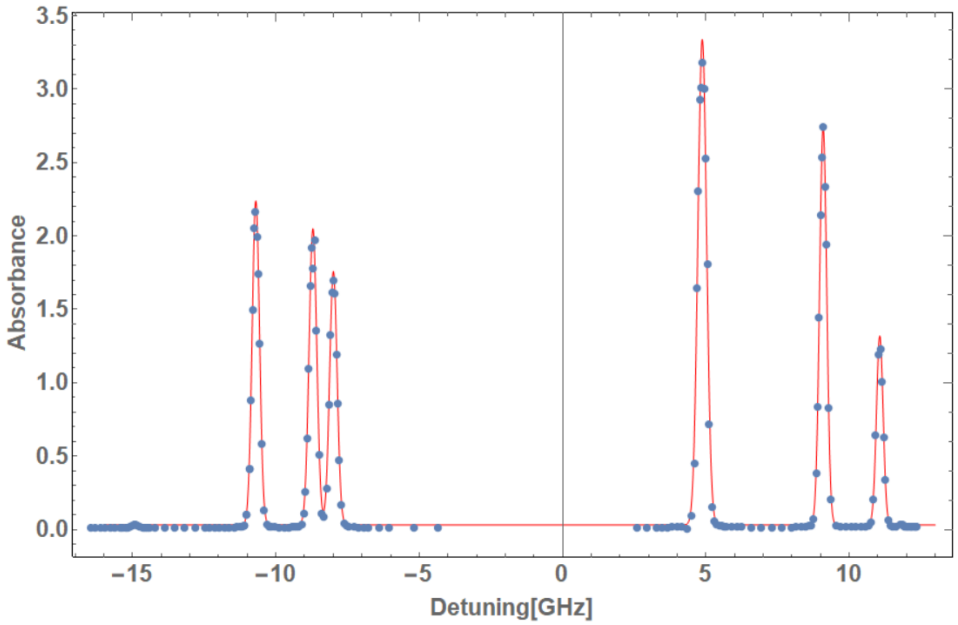

Figure 28: a) Transmittance and b) Absorbance spectrum of iodine as a function of the detuning for 20W green power (sealed cell). The FWHM were estimated to be 250-300MHz.

It is clear that the FWHM of our lines is much smaller than previous measurements with the old cell, and the absorbance has increased as expected. Nevertheless, the FWHM is roughly twice the width we expected due to Doppler broadening at room temperature. This is a cavity effect: due to the different Finesse (and thus number of cavity round-trips) on- and off-resonance, light is more strongly absorbed at the absorption wings than the absorption coefficient there would imply, due to higher number of passes through the cell. On the other hand, on resonance, single-pass absorption is strong, but the number of passes is lower. As a result, the line shapes are wider than the single-pass Doppler-broadened profiles. The detailed theory of this effect is currently under development.

In the absence of pressure broadening, we now succeeded in measuring both quadrupole transitions, the $F = 4 \rightarrow F' = 2$ and $F = 1 \rightarrow F' = 3$, as we see on the outer edges of Figure 28 and, in more detail, in Figure 29.

a)

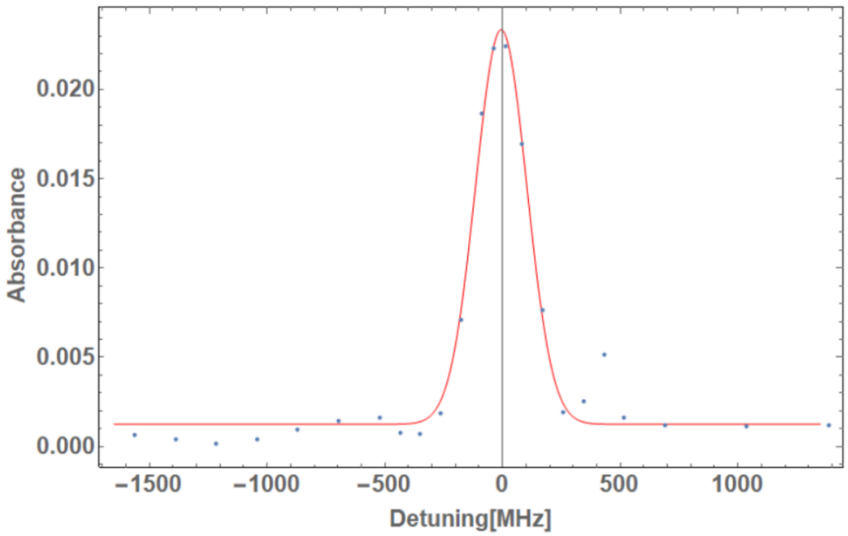

b)

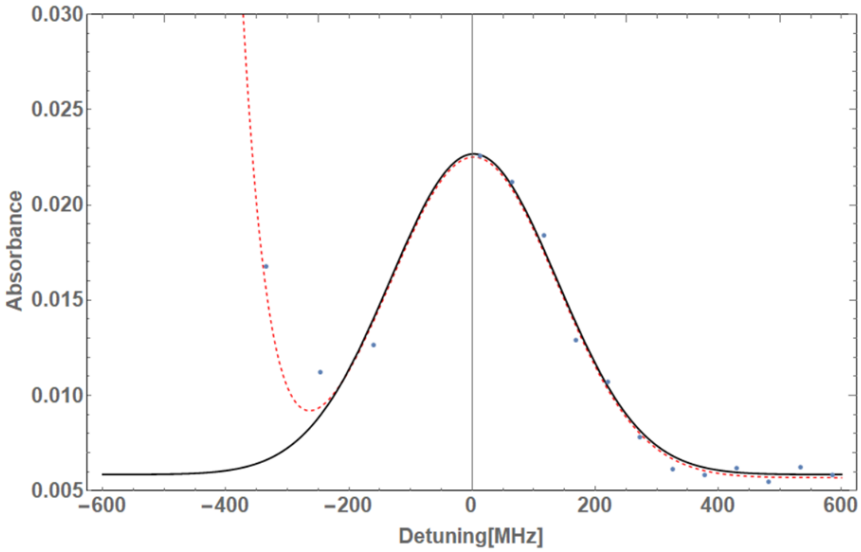

Figure 29:a) The $F = 4$ to $F' = 2$ quadrupole transition absorbance (in absorption-lengths) as a function of the detuning and b) the $F = 1$ to $F' = 3$ quadrupole transition. With the red, dashed line, we represent the sum of the absorption with the adjacent magnetic dipole transition $F = 2$ to $F' = 3$ which appears as an offset in our data.

The absorption of $F = 4$ to $F' = 2$ quadrupole transition is about 2% while for the $F = 1$ to $F' = 3$ is about 0.9% after subtracting the contribution due to the adjacent M1 transition. The ratio of the two absorptions is estimated from the experimental data to be 1.95 ± 0.2, which is within error from the theoretically expected ratio from the Clebsch-Gordan coefficients, 2.14. The electric quadrupole to magnetic dipole ratio parameter, χ, was calculated from our measurements to be $\chi \approx 0.084 \pm 0.01$, which is consistent with preliminary theoretical calculations by our collaborator V. A. Dzuba, $\chi = 0.081$.

6.2.3: Absorption Dependence on Temperature

In order to optimize absorption and maximize the optical depth, we decided to heat the cell in order to increase the density of the molecular iodine. The dependence of the molecular iodine vapor pressure on temperature is shown in the Figure 31 below. As we observe, by increasing the cell temperature by a few degrees Celsius (up to about 60^{o}C), we can increase the vapor pressure of molecular iodine and, as a result its density, tenfold.

Heating the cell was achieved by maintaining the bulk of the cell above the desired target temperature, by wrapping it with heat tapes and applying current, and controlling the pressure by controlling the temperature of a designated *cold spot* on the cell, via a TEC element and a PID temperature controlling circuit. This way we could control the vapor-pressure-defining temperature of the cold-spot to within ~ 0.5 ^{o}C.

a)

b)

Figure 30: a) Iodine cell wrapped with heat tapes in order to increase the temperature. b) A TEC is placed on the iodine reservoir of the cell and is kept at a specific temperature level below the bulk temperature of the cell. This cold spot then defines the molecular iodine vapor pressure inside the cell.

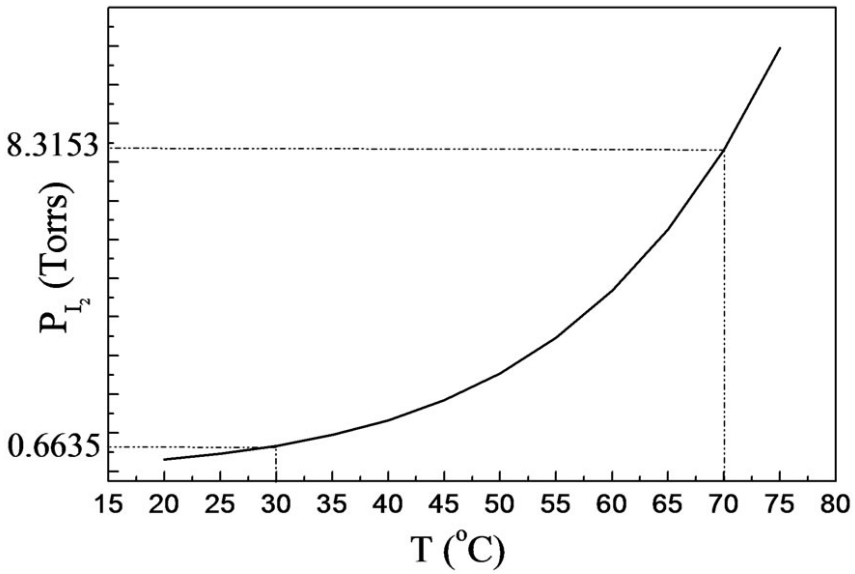

Figure 31: Molecular Iodine vapor pressure as a function of temperature.[11]

The first measurements were of the two quadrupole transitions and their neighboring magnetic dipole transitions at 50 degrees Celsius. The results are shown in Figure 32 and Figure 33 below. From our results we see that we have managed to quadruple absorption from the electric quadrupole transitions relative to the room temperature measurements.

a)

b)

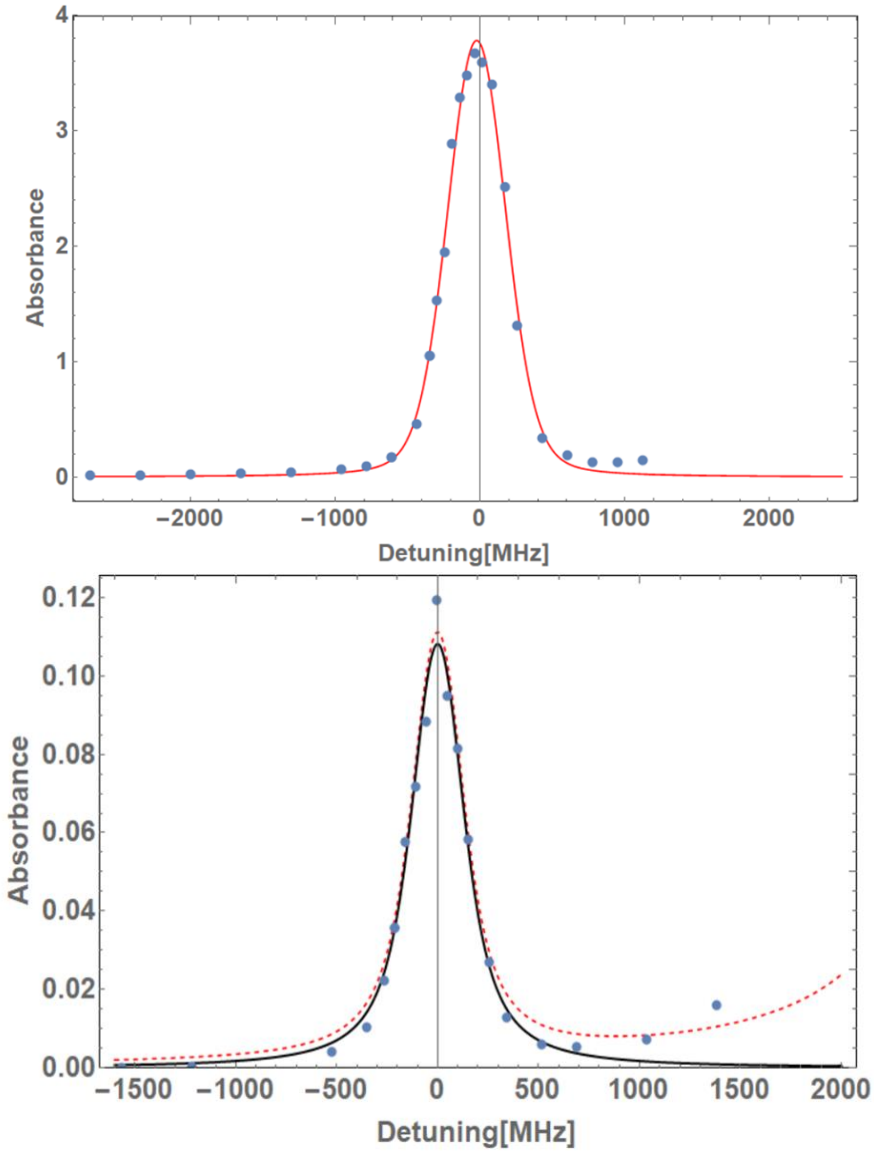

Figure 32:a) The $F = 3$ to $F' = 2$ magnetic dipole transition's absorbance in absorption lengths) as a function of detuning and b) the $F = 4$ to $F' = 2$ quadrupole transition at 50 degrees Celsius. With the red dashed line we represent the sum of the absorption with the adjacent magnetic dipole transition $F = 3$ to $F' = 2$ which appears as an offset in our data.

a)

b)

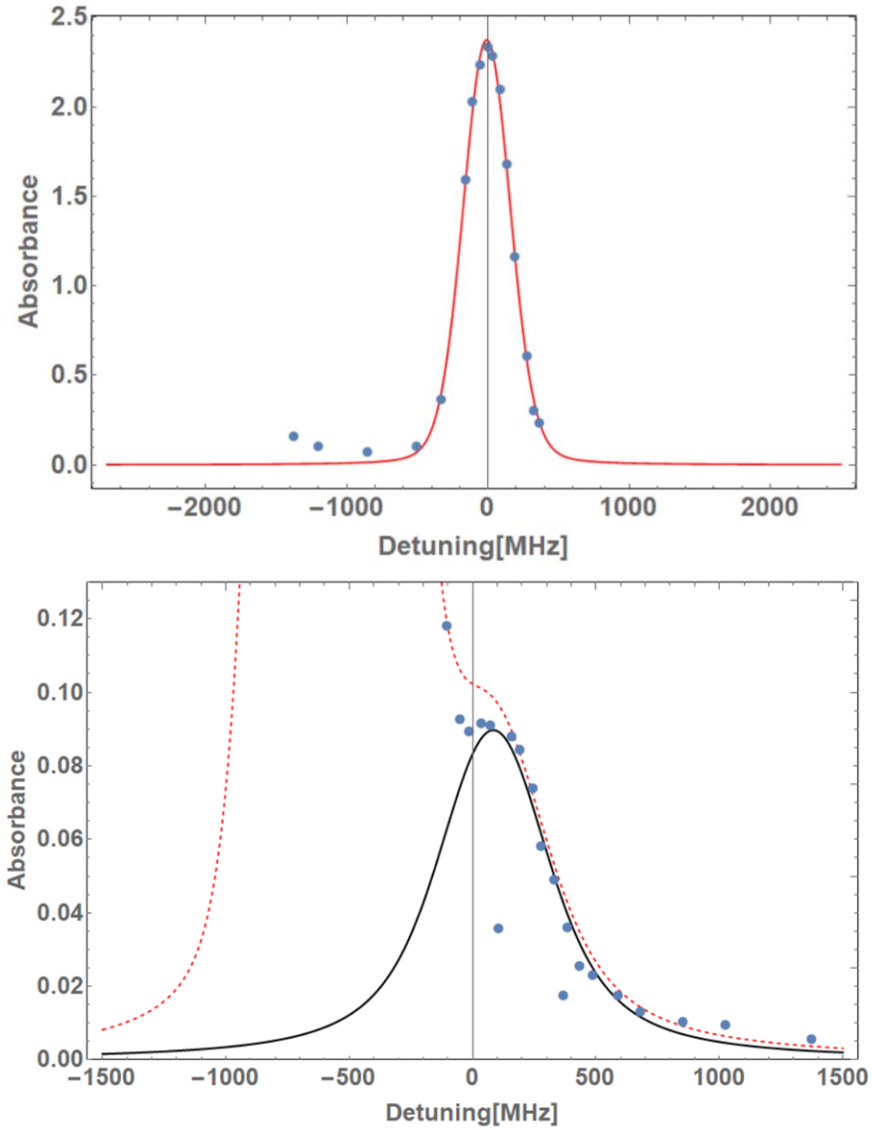

Figure 33:a) The $F = 2$ to $F' = 3$ magnetic dipole transition's absorbance (in absorption lengths) as a function of detuning and b) the $F = 1$ to $F' = 3$ quadrupole transition at 50 degrees Celsius. With the red dashed line, we represent the sum of the absorption with the adjacent magnetic dipole transition $F = 2$ to $F' = 3$ which appears as an offset in our data.

We then measured the transmission of the $F = 4$ to $F' = 2$ quadrupole transition for several temperatures (from lower to significantly higher than room temperature) in order to find the optimum temperature, before pressure broadening becomes significant, which would result in increased homogeneous broadening and reduction in absorption.

a)

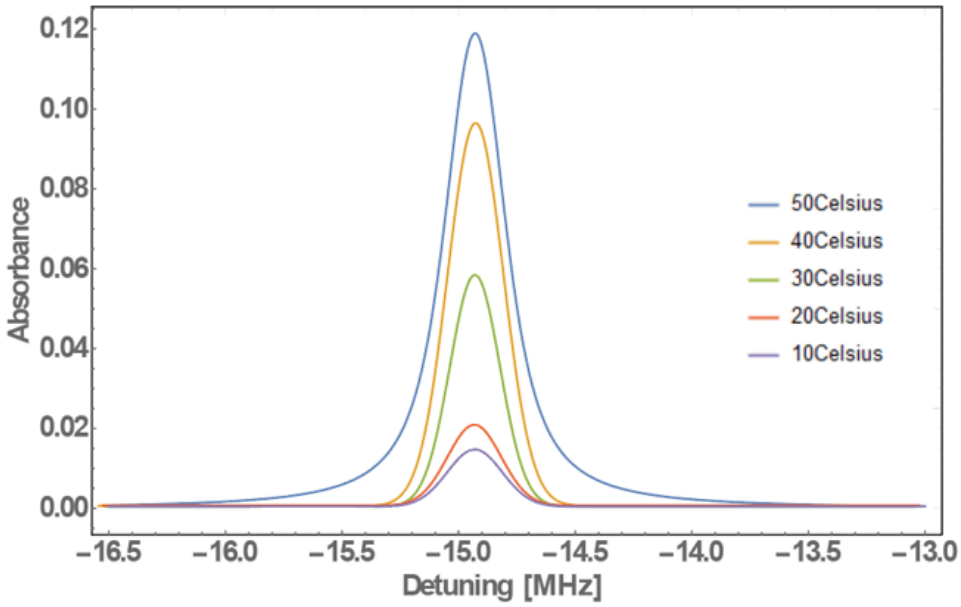

b)

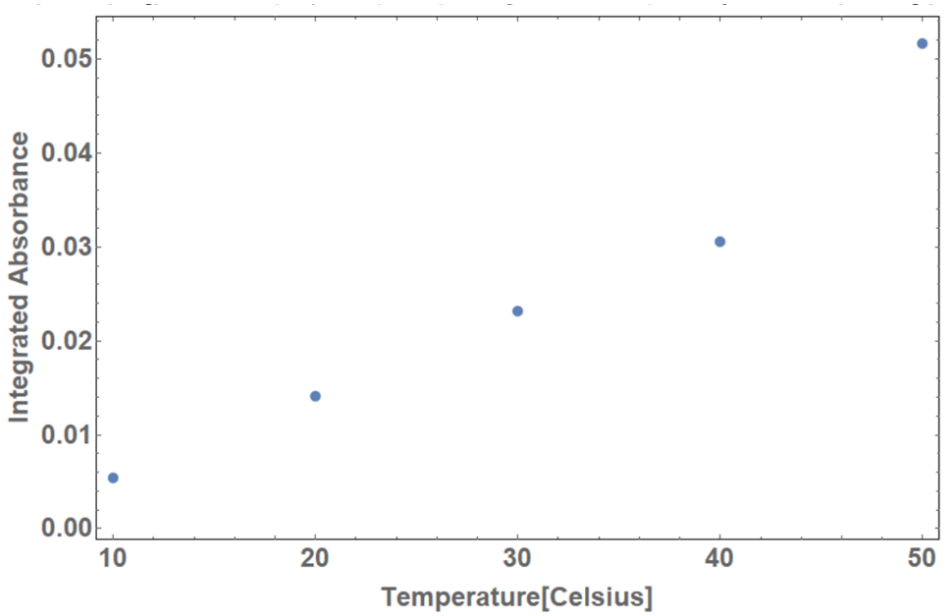

Figure 34: The absorbance of the $F = 4$ to $F' = 2$ quadrupole transition (in absorption lengths) as a function of the detuning from the J=3/2 to J'=1/2 M1nominal transition frequency for various temperatures from 10 to 50 Celsius and b) the integrated absorbance as a function of temperature.

In Figure 34 we see the expected results: the increase in temperature leads to higher densities of atomic iodine and an increase in absorption. The integrated absorption for low temperatures seems to have a linear dependence on temperature, while the width of our lines does not seem to be significantly affected by pressure broadening. Achieving higher temperatures while maintaining stable experimental conditions proved to be a challenge above ~ 55 – 60 ^{o}C at this point and with our experimental setup as described, and work is underway to improve on our apparatus, in order to investigate the practical limits of photodissociation for the production of high atomic iodine densities (given also the fact that our current green laser has, so far, been underutilized, as we have only been using up to about half of its maximum power of 50W). However, the results so far clearly indicate that workable high densities of atomic iodine are achievable, and that we have not yet reached the limits of our production technique.

Conclusions

We have conceived and implemented an optical cavity experimental apparatus for the production of atomic iodine via photodissociation at 532 nm, and the measurement of the IR atomic iodine spectrum at 1315 nm. We combined the atomic theory of iodine absorption with an optical cavity, which led to an increase of the effective interaction path length by a factor equal to the number of passes through the cavity. We improved the conditions of our experiment by constructing a well-performing vacuum-sealed cell and, by increasing the effective cell temperature, we achieved very high atomic iodine densities, which led to a further enhancement in our absorption signals. Still, our apparatus has potential for great improvement, and a clear path to implement these improving steps.

With the above enhancements, we achieved optical depths greater than 10 absorption lengths, which correspond to column densities of about $\rho l \approx 10^{18} - 10^{19}$ cm^{-2}. This high column density of atomic iodine enabled us to measure for the first time the electric quadrupole (E2) component of the, otherwise magnetic-dipole transition $5^2P_{1/2} \rightarrow 5^2P_{3/2}$ at 1315 nm, and determine the electric quadrupole to the magnetic dipole ratio, which we found to be well within agreement with theoretical predictions.

This thesis represents the first steps towards measuring parity non-conservation (PNC) effects in atomic iodine, which manifest as optical activity in this very atomic transition. In theoretical calculations performed for iodine, it has been shown that in order to have a measurable PNC signal, a column density of $\rho l \approx 10^{20} - 10^{21}$ cm^{-2} is required. We believe that achieving such column densities is well within the capabilities of our apparatus, thus the following evolutionary improvements are proposed:

- Improving the cavity finesse, which will increase the number of cavity roundtrips and, therefore, the effective pathlength of the interaction.
- Use a longer cell, which will further increase the effective pathlength.
- Increase the power of the green laser to the currently available 50 W, so that more molecular iodine is photodissociated and higher atomic iodine densities are achieved.
- Improve upon our design regarding heat application and temperature control, so as to allow for stable experimental conditions at higher temperatures, which will, in turn, lead to higher available molecular iodine densities for photodissociation.

Appendix A

A1: Oscillator strength without hyperfine structure

In spectroscopy, oscillator strength is a dimensionless quantity that express the probability of absorption or emission of the electromagnetic radiation in transitions between energy levels of an atom. The oscillator strength can be through of as the ration between the quantum mechanical transition rate and the classical absorption or emission rate of an single electron oscillator with the same frequency as the transition. The oscillator strength f_{ab} of a transition from a lower state $|J_a\rangle$ to an upper state $|J_b$ is defined as:

$$f_{ab} = \frac{2}{3}\frac{m_e\omega_0}{\hbar e^2}\left|\langle j_a|\widehat{\boldsymbol{H_{ab}}}|J_b\rangle\right|^2 \tag{A1}$$

Where $\widehat{\boldsymbol{H_{ab}}}$ is the interaction operator between the states $|a\rangle$ and $|b\rangle$. When the upper state consists of several individuals states , the f-factor is given by a summation over all upper states involved in the transition. If the lower level consists of several states, the f-factor is given by an average over all lower states involved. Hence, for an lower state with degeneracy of g_1 , the f-factor for a transition between degenerate levels can be written as

$$f_{ab} = \frac{2}{3}\frac{m_e\omega_0}{\hbar e^2}\frac{1}{g_1}\sum_{q=-1}^{q=1}\sum_{m_a m_b=1}^{g_1,g_2}\left|\langle j_a m_a|M1_q|J_b m_b\rangle\right|^2 \tag{A2}$$

where $q = 0, \pm 1$ is the summation over all types of polarization[14]. By using the Wigner Eckart theorem we can rewrite *(A2)* as:

$$f_{ab} = \frac{2}{3}\frac{m_e\omega_0}{\hbar e^2}\frac{1}{g_1}\sum_{q=-1}^{q=1}\sum_{m_a m_b=1}^{g_1,g_2}|\langle j_a|M1|J_b\rangle|^2\begin{pmatrix} j_a & 1 & j_b \\ m_a & q & -m_b\end{pmatrix}^2 \tag{A3}$$

But the summations over all m_a, m_b and q calculated to be

$$\sum_{m_a m_b}^{g_1 g_2}\begin{pmatrix} j_a & 1 & j_b \\ m_a & q & -m_b\end{pmatrix}^2 = \frac{1}{3}$$

And

$$\sum_{q=-1}^{q=1}\sum_{m_a m_b}^{g_1 g_2}\begin{pmatrix} j_a & 1 & j_b \\ m_a & q & -m_b\end{pmatrix}^2 = 1$$

Hence, in the case of *a magnetic dipole interaction* of a laser beam with an atomic vapor and assuming that the transition is an isolated $j_a \rightarrow j_b$ line without hyperfine structure, then

$$M1 = \widehat{\boldsymbol{H_{ab}}} = \frac{e}{2m_e c}\langle J_a|\hat{\boldsymbol{L}} + 2\hat{\boldsymbol{S}}|J_b\rangle \tag{A4}$$

and

$$f_{ab} = \frac{2}{3}\frac{m_e\omega_0}{\hbar e^2}\frac{|M1|^2}{(2J_a+1)} \tag{A5}$$

A2: Oscillator strength with hyperfine structure

We must take into account the hyperfine structure. So,

$$f_{ab} = \frac{2}{3}\frac{m_e\omega_0}{\hbar e^2}\sum_{q=-1}^{q=1}\sum_{\substack{F_a,F_b\\ m_a,m_b}}\frac{1}{g_1}\langle F_a m_a|M1_q|F_b m_b\rangle^2 \tag{A6}$$

$$= \frac{2}{3}\frac{m_e\omega_0}{\hbar e^2}\sum_{q=-1}^{q=1}\sum_{\substack{F_a,F_b\\ m_a,m_b}}\frac{1}{g_1}\langle F_a|M1_q|F_b\rangle^2\begin{pmatrix}F_b & 1 & F_a\\ -m_b & q & m_a\end{pmatrix}^2 \Rightarrow$$

$$f_{ab} = \frac{2}{3}\frac{m_e\omega_0}{\hbar e^2}\sum_{F_aF_b}\frac{1}{g_1}\langle F_a|M1_q|F_b\rangle^2$$

Now, if we use equation *(3.16)* we get

$$f_{ab} = \frac{2m_e\omega_0}{\hbar e^2}\frac{\langle j_a|M1|j_b\rangle^2}{3}\sum_{F_a,F_b}\frac{(2F_a+1)(2F_b+1)}{2F_a+1}\begin{Bmatrix}j_a & k & j_b\\ F_b & I & F_a\end{Bmatrix}^2 \tag{A7}$$

And by substituting in the equation *(3.14)* we get the refractive index witch is given by equations *(3.19)*, *(3.20)*.

A3: Oscillator strength with Quadrupole interaction

To include it in the refractive index, we make the substitution

$$\frac{M1}{3} \to \left\langle j_a\left|\mu_q^{(1)} - \frac{q\omega}{4\sqrt{3}}Q_q^{(2)}\right|j_b\right\rangle$$

Introducing the electric quadrupole to magnetic dipole ratio parameter

$$\chi = \frac{\omega}{4\sqrt{3}}\frac{\langle j_a|Q^{(2)}|j_b\rangle}{\langle j_a|\mu^{(1)}|j_b\rangle}$$

Hence,

$$f_{ab} = \frac{2}{3}\frac{m_e\omega_0}{\hbar e^2}\sum_{q=-1}^{q=1}\sum_{\substack{F_a,F_b\\ m_a,m_b}}\frac{1}{g_1}\left\langle F_a m_a\left|\mu_q^{(1)} - \frac{q\omega}{4\sqrt{3}}Q_q^{(2)}\right|F_b m_b\right\rangle^2 \tag{A8}$$

$$= \frac{2}{3}\frac{m_e\omega_0}{\hbar e^2}\sum_{q=-1}^{q=1}\sum_{\substack{F_a,F_b\\ m_a,m_b}}\frac{1}{g_1}\Big(\left\langle F_a m_a\left|\mu_q^{(1)}\right|F_b m_b\right\rangle^2$$

$$- 2\left\langle F_a m_a\left|\mu_q^{(1)}\right|F_b m_b\right\rangle\left\langle F_a m_a\left|\frac{q\omega}{4\sqrt{3}}Q_q^{(2)}\right|F_b m_b\right\rangle + \left\langle F_a m_a\left|\frac{q\omega}{4\sqrt{3}}Q_q^{(2)}\right|F_b m_b\right\rangle^2\Big)$$

$$= \frac{2}{3}\frac{m_e\omega_0}{\hbar e^2}\sum_{q=-1}^{q=1}\sum_{\substack{F_aF_b\\ m_a,m_b}}\frac{1}{g_1}\left(\left\langle F_a\left|\mu^{(1)}\right|F_b\right\rangle^2\begin{pmatrix}F_a & 1 & F_b\\ -m_a & q & m_b\end{pmatrix}^2\right.$$
$$\left.+\left\langle F_a\left|\frac{\omega}{4\sqrt{3}}Q^2\right|F_b\right\rangle^2\right)\begin{pmatrix}F_a & 2 & F_b\\ -m_a & q & m_b\end{pmatrix}^2$$

But for the summation over m_a, m_b and q we have,

$$\sum_{q=-1}^{q=1}\sum_{m_am_b}^{g_1g_2}\begin{pmatrix}F_a & 1 & F_b\\ m_a & q & -m_b\end{pmatrix}^2 = 1$$

$$\sum_{q=-1}^{q=1}\sum_{m_am_b}^{g_1g_2}\begin{pmatrix}F_a & 2 & F_b\\ m_a & q & -m_b\end{pmatrix}^2 = \frac{3}{5}$$

Hence,

$$f_{ab} = \frac{2}{3}\frac{m_e\omega_0}{\hbar e^2}\sum_{F_a,F_b}\frac{1}{g_1}\left(\left\langle F_a\left|\mu^{(1)}\right|F_b\right\rangle^2 + \frac{3}{5}\left\langle F_a\left|\frac{\omega}{4\sqrt{3}}Q^2\right|F_b\right\rangle^2\right) \tag{A9}$$

$$= \frac{2}{3}\frac{m_e\omega_0}{\hbar e^2}\sum_{F_a,F_b}\frac{(2F_a+1)(2F_b+1)}{2F_a+1}\left(\left\langle j_a\left|\mu^{(1)}\right|j_b\right\rangle^2\begin{Bmatrix}j_a & 1 & j_b\\ F_b & I & F_a\end{Bmatrix}^2\right.$$
$$\left.+\frac{3}{5}\left\langle j_a\left|\frac{\omega}{4\sqrt{3}}Q^2\right|j_b\right\rangle^2\begin{Bmatrix}j_a & 2 & j_b\\ F_b & I & F_a\end{Bmatrix}^2\right)$$

$$f_{ab} = \frac{2m_e\omega_0}{\hbar e^2}\frac{\left\langle j_a\left|\mu^{(1)}\right|j_b\right\rangle^2}{3}\sum_{F_a,F_b}\frac{(2F_a+1)(2F_b+1)}{2F_a+1}\left(\begin{Bmatrix}j_a & 1 & j_b\\ F_b & I & F_a\end{Bmatrix}^2\right. \tag{A10}$$
$$\left.+\frac{3}{5}x^2\begin{Bmatrix}j_a & 2 & j_b\\ F_b & I & F_a\end{Bmatrix}^2\right)$$

So, the refractive index can be rewritten as equation *(3.24), (3.25).*

References

1. Verdeyen, J. T., Thomas, J. & Verdeyen, I. J. T. *Laser Electronics THIRD EDITION*.
2. Anderson, D. Z. Alignment of resonant optical cavities. *Appl. Opt.* **23**, 2944 (1984).
3. Bougas, L., Katsoprinakis, G. E., Von Klitzing, W. & Rakitzis, T. P. Cavity-Enhanced Parity-Nonconserving Optical Rotation Scheme for measurements in Xe, Hg and I. 1–12 (2013).
4. Lambropoulos, P. & Petrosyan, D. Fundamentals of quantum optics and quantum information. *Fundam. Quantum Opt. Quantum Inf.* 1–325 (2007) doi:10.1007/978-3-540-34572-5.
5. Dommelen, L. Van. Physics - Quantum Mechanics - Engineers. 1623 (2012).
6. Sobelman, I. I. AtonllC Spectra and Radidtive Transitions. **1**,.
7. Fitzpatrick, R. *Quantum Mechanics*. (2015). doi:https://doi.org/10.1142/9789814689991_0008.
8. Libbrecht, K. G. & Libbrecht, M. W. Interferometric measurement of the resonant absorption and refractive index in rubidium gas. *Am. J. Phys.* **74**, 1055–1060 (2006).
9. Almog, I. F., Bradley, M. S. & Bulovi, V. Lorentz model. *MIT OpenCourseWare* 1–34.
10. Katsoprinakis, G. E., Chatzidrosos, G., Kypriotakis, J. A., Stratakis, E. & Rakitzis, T. P. High steady-state column density of I(2P3/2) atoms from I2 photodissociation at 532 nm: Towards parity non-conservation measurements. *Sci. Rep.* **6**, 6–13 (2016).
11. Ip, J. K. K. & Burns, G. Recombination of iodine atoms by flash photolysis over a wide temperature range. II i2 in He, Ar, Xe, N2, CO. *J. Chem. Phys.* **56**, 3161–3164 (1972).
12. Bougas, L. Cavity-enhanced Polarimetry: Applications in Atomic Parity Violation & Molecular Chirality. *P H DThesis* (2013).
13. Deng, L. hua, Li, X. yun, Zhu, Y. yue & Chen, Y. qin. Hyperfine structure near infrared spectrum of atomic iodine. *J. Quant. Spectrosc. Radiat. Transf.* **161**, 153–156 (2015).
14. Axner, O., Gustafsson, J. O., Omenetto, N. & Winefordner, J. D. Line strengths, A-factors and absorption cross-sections for fine structure lines in multiplets and hyperfine structure components in lines in atomic spectrometry - A user's guide. *Spectrochim. Acta - Part B At. Spectrosc.* **59**, 1–39 (2004).